

NASA TN D-341



111-25
100-607
201

TECHNICAL NOTE

D-341

EXPERIMENTAL INVESTIGATION OF A HYPERSONIC
GLIDER CONFIGURATION AT A MACH NUMBER OF
6 AND AT FULL-SCALE REYNOLDS NUMBERS

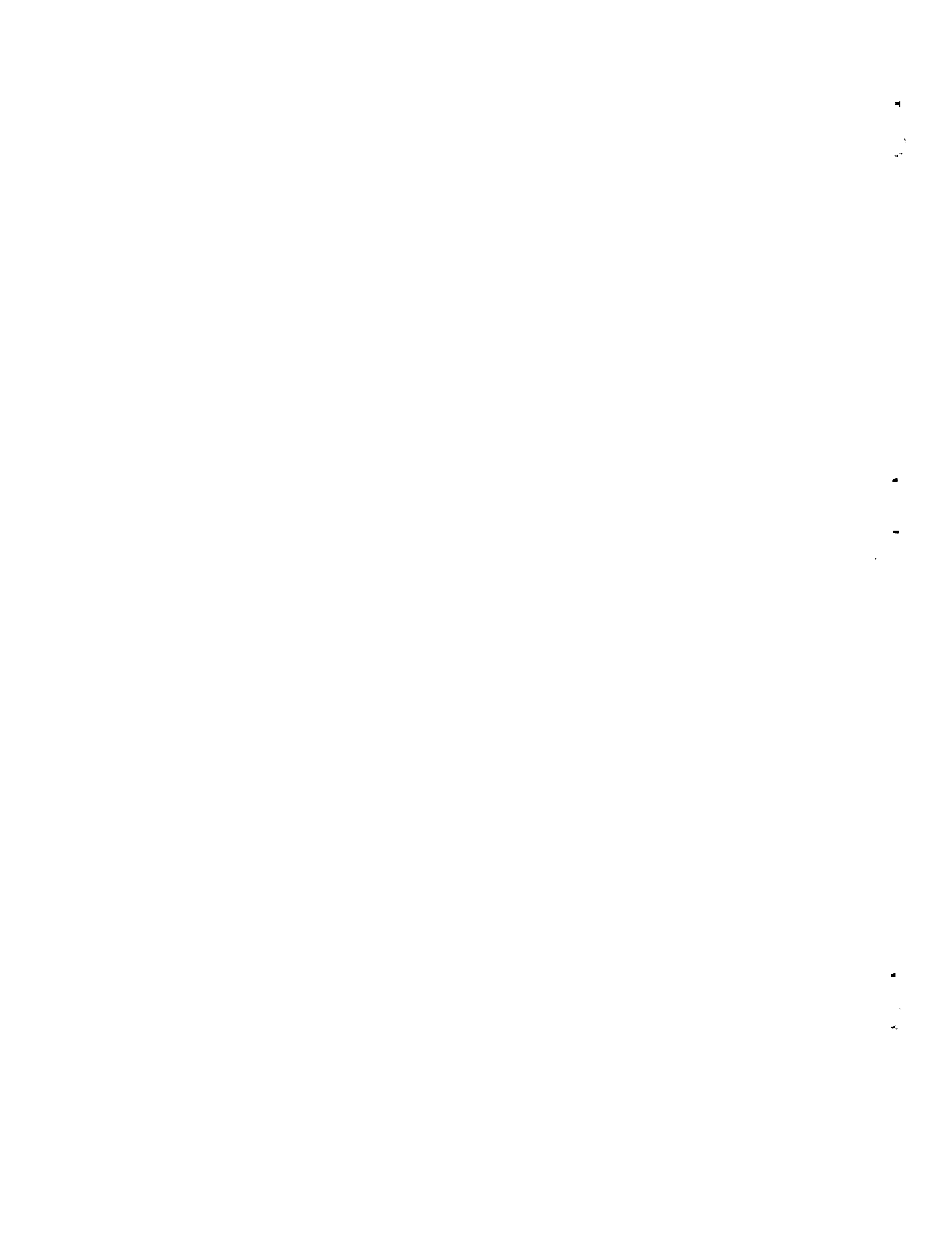
By Alvin Seiff and Max E. Wilkins

Ames Research Center
Moffett Field, Calif.

PROPERTY
OF
GODDARD SPACE FLIGHT CENTER
LIBRARY

NATIONAL AERONAUTICS AND SPACE ADMINISTRATION
WASHINGTON

January 1961



NATIONAL AERONAUTICS AND SPACE ADMINISTRATION

TECHNICAL NOTE D-341

EXPERIMENTAL INVESTIGATION OF A HYPERSONIC
GLIDER CONFIGURATION AT A MACH NUMBER OF
6 AND AT FULL-SCALE REYNOLDS NUMBERS

By Alvin Seiff and Max E. Wilkins

SUMMARY

The aerodynamic characteristics of a hypersonic glider configuration, consisting of a slender ogive cylinder with three highly swept wings, spaced 120° apart, with the wing chord equal to the body length, were investigated experimentally at a Mach number of 6 and at Reynolds numbers from 6 to 16 million. The objectives were to evaluate the theoretical procedures which had been used to estimate the performance of the glider, and also to evaluate the characteristics of the glider itself. A principal question concerned the viscous drag at full-scale Reynolds number, there being a large difference between the total drags for laminar and turbulent boundary layers.

It was found that the procedures which had been applied for estimating minimum drag, drag due to lift, lift curve slope, and center of pressure were generally accurate within 10 percent. An important exception was the nonlinear contribution to the lift coefficient which had been represented by a Newtonian term. Experimentally, the lift curve was nearly linear within the angle-of-attack range up to 10° . This error affected the estimated lift-drag ratio.

The minimum drag measurements indicated that substantial amounts of turbulent boundary layer were present on all models tested, over a range of surface roughness from 5 microinches maximum to 200 microinches maximum. In fact, the minimum drag coefficients were nearly independent of the surface smoothness and fell between the estimated values for turbulent and laminar boundary layers, but closer to the turbulent value. At the highest test Reynolds numbers and at large angles of attack, there was some indication that the skin friction of the rough models was being increased by the surface roughness. At full-scale Reynolds number, the maximum lift-drag ratio with a leading edge of practical diameter (from the standpoint of leading-edge heating) was 4.0.

The configuration was statically and dynamically stable in pitch and yaw, and the center of pressure was less than 2-percent length ahead of the centroid of plan-form area.

A method of analyzing a free-flight time and distance history to define the drag for the case of large in-flight variations in drag due to lift was developed and applied and is described in the report.

INTRODUCTION

Analytical studies of hypersonic gliders are frequently limited by the present state of knowledge of aerodynamics, particularly for complete configurations in which wings, bodies, and stabilizing surfaces interact. Exactly applicable theories usually do not exist, and intuitive and approximate methods must be employed. This was the case in the analysis of the example configuration of reference 1.

Reference 1 was concerned with an airplane or glider design for high supersonic or hypersonic Mach numbers which are still well below satellite speed. For such a case, aerodynamic efficiency, as measured by the lift-drag ratio, retains the importance which it has always had in lower speed aircraft in that it determines the glide range, thrust-weight ratio for steady flight, etc. The example configuration of reference 1 was selected, after a consideration of generally desirable features for such aircraft, to illustrate the levels of aerodynamic efficiency and aerodynamic heating that might be expected. The configuration selected, which is illustrated in figure 1, appeared to be favorable from these standpoints and also with respect to aerodynamic stability, and so it was decided to investigate its performance experimentally in the Ames Supersonic Free-Flight Wind Tunnel. That investigation is the subject of the present report.

The experiments were intended to evaluate both the performance of the configuration and the methods of calculation used to estimate its performance. They were further intended to provide information on the state of the boundary layer under conditions approximating those of full-scale flight. The tests were conducted at a Mach number of 6 and the Reynolds numbers, from 6 to 16 million, extended up to and beyond the full-scale values given in reference 1. The temperature conditions of the boundary layer also approximated those for flight in the atmosphere in that the model surface temperature was low compared to the boundary-layer recovery temperature. The characteristics investigated in the tests included minimum drag, for smooth and roughened surfaces, drag due to lift, lift-curve slope, and static and dynamic stability in pitch and yaw.

In addition to the experiments, further estimates beyond those given in reference 1 of the aerodynamic drag of the configuration were made, incorporating some refinements which were judged unnecessary for purposes of the original analysis. (It should be noted that these refinements did not in all cases improve the accuracy of the estimates.) Furthermore,

since the methods used to estimate the drag were not described in detail in reference 1, they are described herein so as to permit the reader to understand fully the methods employed and the accuracy obtained.

Earlier experiments in a supersonic wind tunnel with a configuration derived from that of reference 1 were reported in reference 2. Those tests were made at generally lower Reynolds numbers than the present tests and at the temperature condition for zero heat transfer. In addition, the configuration was modified from that originally suggested by being cut off at about the 3/4 point of its length. The results reported are compared with those obtained herein.

Another related wind-tunnel investigation is reported in reference 3. There, some modifications of the present configuration were made to improve further its aerodynamic efficiency while retaining its apparently desirable aerodynamic stability features. At a Mach number of 3.3 and a Reynolds number of 5.5 million, a lift-drag ratio of 6.7 (without base drag) was then obtained experimentally, and the aerodynamic stability for combined attitudes of pitch and yaw appeared to be very satisfactory. These data are the most complete available at supersonic speeds with respect to the stability characteristics of this type of configuration. At subsonic speeds, similarly desirable characteristics were observed and reported in references 4 and 5.

SYMBOLS

A	reference area, projected plan-form area including body, ft ²
$\frac{A_T}{A_W}$	ratio of total surface area with turbulent flow to total wetted area, dimensionless
b	span of a wing panel, measured to body axis, ft
C_D	drag coefficient, $\frac{\text{total drag}}{q_\infty A}$
C_{D_b}	base drag coefficient
$C_{D_{cyl}}$	foredrag coefficient of a circular cylinder normal to the stream
$C_{D_{eff}}$	effective drag coefficient, see equations (A7) and (A8)
C_{D_F}	skin-friction drag coefficient
C_{D_i}	interference pressure drag on wings

C_{D_0}	drag coefficient at zero angle of attack	
C_{D_p}	pressure drag coefficient	
C_F	average skin-friction coefficient	
C_L	lift coefficient, $\frac{\text{lift}}{q_\infty A}$	
C_{L_0}, C_{Y_0}	trim lift and side-force coefficients	
C_{L_α}	lift-curve slope, per radian	
$\overline{C_{L_\alpha}}$	average lift-curve slope given by linear analysis of a nonlinear lift curve	A 2 4 0
C_m	pitching-moment coefficient, $\frac{\text{pitching moment}}{q_\infty A l}$	
C_{m_α}	pitching-moment-curve slope, per radian	
$C_{m_q} + C_{m_{\dot{\alpha}}}$	damping-in-pitch derivative, $\frac{\partial C_m}{\partial q(l/v)} + \frac{\partial C_m}{\partial \dot{\alpha}(l/v)}$	
C_{N_α}	normal-force-curve slope	
d	body cylinder diameter, ft	
I_y	transverse moment of inertia, $m\sigma^2$, slug-ft ²	
K	constant, $\frac{\rho A}{2m}$, ft ⁻¹	
$K_{1,2,3}$	constants in equation (A13), deg	
k	constant in equation (A3)	
$\frac{L}{D}$	lift-drag ratio	
l	body length, ft	
M	Mach number	
M_N	component of Mach number normal to wing leading edge	
m	mass of model, slugs	
$\frac{p_b}{p_\infty}$	ratio of base pressure to free-stream static pressure	
p	roll rate, radians/ft	
q_∞	free-stream dynamic pressure, lb/ft ²	

q	pitching rate, radians/sec
R_{∞}	Reynolds number based on free-stream air properties and model length
V	velocity of model with respect to the air stream, ft/sec
x	distance along flight path measured relative to a point fixed in the air stream, ft
x	distance from model tip (before blunting), ft
x_{cg}	distance from model tip to center of gravity, ft
x_{cp}	distance from model tip to center of pressure, ft
x_t	streamwise distance from wing leading edge to transition point, ft
x_{α}, x_{β}	distance ahead of the first shadowgraph station at which zero phase angle occurs in the pitch and yaw oscillations, respectively, ft (eq. (A9))
y	horizontal coordinate normal to the flight path, ft
z	coordinate normal to the flight path and the y-axis, ft
α	angle of attack (angle between model axis and resultant wind direction projected onto the vertical plane)
α_m, β_m	amplitude of oscillation in pitch and yaw, respectively
α_r	resultant angle of attack, $\sqrt{\alpha^2 + \beta^2}$
$\overline{\alpha_r^2}$	mean square resultant angle of attack, $\frac{\int_0^x \alpha_r^2 dx}{x}$
β	angle of sideslip (angle between model axis and resultant wind direction projected onto the horizontal plane)
β	$\sqrt{M^2 - 1}$
$\eta_{1,2}$	damping exponents in equation (A13), ft^{-1}
Λ	leading-edge sweepback angle, deg
λ	wave length of pitching oscillation with respect to the air stream, ft
ξ	dynamic stability parameter, $C_D - C_{I\alpha} + (C_{m\dot{q}} + C_{m\dot{\alpha}}) (l/\sigma)^2$, dimensionless

ρ	air density, slugs/ft ³
σ	transverse radius of gyration, ft
θ, ψ, φ	attitude coordinates of the model relative to earth-fixed axes
$\omega_{1,2}$	rates of rotation of complex vectors which generate the model pitching motion, radians/ft (eq. (A13))

All angles are in radians except where otherwise noted.

Superscripts

($\dot{}$)	derivative with respect to time
(\prime)	derivative with respect to distance

Subscripts

Except where otherwise defined, the following subscripts apply:

i	initial conditions
∞	free-stream conditions
B	body
W	wing
L	laminar
T	turbulent
le	leading edge
n	body nose or tip

DESCRIPTION OF TESTS

Test Technique and Test Conditions

A
2
4
0

Models of the geometry shown in figure 1 were tested in free flight by launching them in sabots (figs. 2(a), (b), and (c)) from a 1.75-inch smooth bore gun at a nominal velocity of 3350 feet per second into the test section of the Supersonic Free-Flight Wind Tunnel (ref. 6). The supersonic air stream of the wind tunnel, flowing at a nominal speed of 1660 feet per second and a nominal Mach number of 2 opposite to the flight direction of the model, gave a resultant air velocity relative to the model of about 5000 feet per second, corresponding to a Mach number of 6. Wind-tunnel reservoir pressures ranged from 17 to 65 psig, corresponding to test-section static pressures of about 4 to 10 psia and length Reynolds numbers of from 6 to 16 million. The nominal static temperature of air in the test section was 295° Rankine; the models were at room temperature before firing and at temperatures slightly above room temperature during the test.

The trajectory of the model through the test section was recorded over a 24-foot length in shadowgraph stations located 3 feet apart. Each station recorded side- and plan-view shadowgraphs along with reference marks from which x , y , z , θ , and ψ coordinates could be read, the linear coordinates with accuracy within 0.003 inch, and the angles within 0.07° . The θ and ψ angles were read relative to earth-fixed direction references. Correction for the angle between the resultant wind direction and the earth-fixed reference directions gave values of α and β . In addition, roll angle could be obtained from the projected positions of the model fin tips, one of which was clipped (see fig. 1) to make positive orientation possible, and time was recorded in a precision chronograph with an accuracy of 0.03 microsecond.

The trajectory data were analyzed to obtain drag coefficient (from the deceleration in flight), lift coefficient (from the swerving motion of the center of gravity), static stability (from the pitching frequency), and damping in pitch (from the diminution of pitch amplitude). The methods used to analyze the data are given in appendix A, and the corrections applied to the data for deviations from standard or nominal model geometry, Mach number, and Reynolds number are described in appendix B and table I. Representative shadowgraph pictures of the models in flight are given in figure 3. Inset on each picture is a vector showing the free-stream direction and a diagrammatic rear view of the model showing its roll orientation relative to the y and z axes.

Models

Fabrication.- The models were centrifugally cast from aluminum alloy 356 to economically provide the large number needed. The castings were heat treated to T6 designation, after which the base of the models was faced off flat and the ballast hole drilled (fig. 1). This hole accommodated a screw made of Fansteel No. 77 (weight 0.60 lb/in³) to move the center of gravity forward. The sides of the wings were filed or machined to remove the imperfections of the casting and to obtain a flat wing surface. The wing leading edges were filed flat and the width of the flat was measured with a machinists microscope. The model was then finished to the desired degree of smoothness, and the leading edges were rounded to approximate a hemicylinder. A magnesium screw was inserted in the base hole to aid in the measurement of angle of attack from the shadowgraph pictures.

Surface finish.- Two types of surface finish were desired - one sufficiently smooth to eliminate transition due to roughness and thus obtain the maximum amount of laminar flow; the other, rough enough to cause total turbulent flow. Four different types of finish were employed on the smooth models: The maximum surface roughnesses were 5 microinches, 10 to 20 microinches, 30 to 35 microinches, and 60 to 90 microinches. The polishing agents used to produce these finishes were 0 to 1/2 micron diamond polish, 3/0 emery polishing paper, 600 silicon carbide paper, and 320 silicon carbide paper. Surfaces representative of these finishes have been shown in the photomicrographs of reference 7. The rough models were finished with a coarse grade of emery cloth designated 1/0 which produced random scratches (measured to be 100 to 200 microinches deep) over the surface. These scratches would correspond, on a full-scale airplane 50 feet long, to scratches from 0.020 to 0.040 inch deep. Additional roughness in the vicinity of the leading edge was given to some of the rough-surfaced models by sandblasting, filing notches in the wing leading edge, or by using a sharp-pointed punch (0.006-inch tip radius) held at an angle of about 60° to the surface and pushed into the metal to gouge up burrs. The punch marks are visible along the leading edges of the model in figure 2(a), as are the roughness scratches over the entire surface. (Fig. 2(b), on the other hand, is representative of a smooth model, and has finer polishing scratches longitudinally oriented.) In figure 2(c), there is shown a roughened model with a sandblasted strip about 0.1 inch wide along its leading edge. The sandblasting was done with carborundum grit and produced pits and burrs about 500 microinches high measured from the original surface level. Photomicrographs of a roughness element 0.006 inch high produced by the punch are shown in figures 2(d) and (e). A photomicrograph of a profile of a notch filed in the wing leading edge is shown in figure 2(f).

Sabots

Two different sabot types were used to launch the models - one for high angle of attack tests (over 60°), and the other for low-angle tests. The one intended for high angles is shown in figure 2(a) and consisted of three lucite fingers to align the model in the gun, an aluminum pusher plate to distribute the launching force from the model base into the plastic, and a nylon sealing plug. The sabot was not often successful because the model received too severe a disturbance from the sabot on separation, causing its flight path to move completely out of the field of view of the shadowgraph stations. The other sabot shown in figures 2(b) and (c) consisted of three pieces to which the model was secured by means of a screw attached to the model base. A hole drilled through the sabot allowed powder gases inside the sabot, which on emerging from the gun muzzle would separate the three sabot pieces from the model. This sabot was quite successful in obtaining low-angle data. Efforts to alter this sabot to produce high-angle data were not rewarding.

ESTIMATE AND DISCUSSION OF THE MINIMUM DRAG COEFFICIENT

This section of the report describes the methods used to estimate the minimum drag and discusses the relative contributions of the various drag-producing elements of the configuration. Readers who are not particularly interested in these aspects can skip this part and go directly to the Results and Discussion without loss of continuity.

Methods Used to Estimate Drag Components

Drag of the blunt (hemicylindrical) leading edge.- From crossflow theory (flow component normal to the leading edge assumed independent of that parallel to the leading edge) or Newtonian theory, the following equation for drag coefficient of the leading edge can be obtained.

$$C_{D_{l_e}} = C_{D_{cyl}} \frac{l_{l_e} d_{l_e}}{A} \cos^3 \Lambda \quad (1)$$

Here $C_{D_{cyl}}$ is the drag coefficient of the hemicylinder at the crossflow Mach number (crossflow theory), $4/3$ (Newtonian theory), or $2/3$ the pitot pressure coefficient (modified Newtonian theory). Penland (ref. 8) shows that the crossflow theory works very well for sweepback angles of 60° and less, but that three-dimensional effects are important at 75° sweepback. Hence, for greatest accuracy, the crossflow theory was used in the present

estimates with values of $C_{D_{cyl}}$ measured on a leading edge with 75° sweep-back (from ref. 8). The foredrag values obtained from reference 8 showed a variation in $C_{D_{cyl}}$ from 1.20 to 1.24 over the range of Mach numbers encountered in the present tests.

Pressure drag of the wing upper and lower surfaces.- The pressure drag of the upper and lower surfaces of the wings was calculated in two parts - that due to thickness and that due to wing-body interference. The thickness drag was estimated from the flow deflection angle in the streamwise direction by use of the charts for wedge flow. (Because of the high degree of leading-edge sweep, the blunt leading edge was assumed not to affect the average pressure over the surface of the wing.) The pressure drag obtained was almost negligible because of the small flow deflection angle (0.5°) and the small frontal area. It is shown in figure 4(a), where it is designated "basic pressure drag, wings" and appears as about one pencil-line width at the scale of the graph.

A
2
4
0

The wing is also immersed in the pressure field generated by the body nose. The flow fields around several pointed ogives at high supersonic speeds were calculated by the authors of reference 9 by the method of characteristics, and their solutions were available. (The small amount of tip bluntness present on the test models was assumed to have negligible effect on the pressure field.) It was observed from these solutions, for cases close to the present case, that the isobars in the disturbed flow field were approximately straight Mach lines extending from the body surface at the local Mach angle. From this observation, the body surface pressures for the $l/d = 5$ ogive at a Mach number of 6 were used to calculate the pressure distribution in the surrounding field.

The interference pressures calculated in this way are shown in figure 5, and near the leading edge they were considerably larger than the thickness pressures. However, there is also a region of favorable interference as shown in the figure. The interference pressure drag, integrated from this pressure distribution, was four times as large as the thickness pressure drag, and was combined linearly with the thickness pressure drag. It is shown in figure 4(a).

Pressure drag of the body nose.- The pressure drag of the ogival nose was taken from the correlated characteristics solutions of reference 10. Correction was made for the slightly blunted (hemispherical) tip by allowing a tip drag coefficient of 0.9 based on tip frontal area and subtracting out the drag of the conical tip which it replaced. The fraction of the nose frontal area which is masked by the wing panels (about 15 percent) was accounted for by a proportionate reduction in pressure drag coefficient.

Skin friction.- The skin-friction drag of the wing panels and the body could not be calculated rigorously because of a number of complications. These include interaction of the wing and body boundary layers

at the wing root; interaction of the boundary layers with shear layers which result from nose and leading-edge bluntness; and three-dimensional flow effects in the boundary layers. Approximate calculations were made in which it was attempted to include first-order effects of the above complications.

A
2
4
0

In the case of the wing panels, the flat-plate boundary-layer theories of references 11 (laminar) and 12 (turbulent) were used with the following modifications. The variation in chord Reynolds number with spanwise position was treated by the method noted briefly in footnote 8 of reference 1. The air properties at the boundary-layer edge were assumed to be defined by the mean static pressure on the wing (including interference pressure) and the total pressure downstream of a conical shock wave of 17° semiapex angle, a shock wave which approximates the shock envelope of the test model. The effects of the pressure gradient due to body-wing interference were neglected.

The local dynamic pressure was raised by body-wing interference to a level which was, on the average, about 20 percent greater than in the free stream and which caused an increase in the estimated skin-friction drag of the wing panels by about 15 percent over that which would be obtained in the absence of the body. In fact, the principal effect of the body-wing interference was to increase the skin-friction estimates on the wing panels, especially in the case of a turbulent boundary layer. The skin-friction estimates for the wing panels are shown in figure 4.

The skin friction of the body also was calculated from flat-plate theories, the justification for this being the slenderness of the body and the data given in reference 13. The body area covered by the root sections of the wing panels was subtracted from the total body surface area. The estimate of the body skin friction is shown in figure 4, and the total estimated skin friction is shown to an enlarged scale in figure 6 for laminar and turbulent boundary layers.

Base drag.- The estimate of base drag was necessarily based on correlations of experimental data and was uncertain because there is very little data available for Mach numbers greater than 4. Data on effects of Reynolds number for laminar and turbulent boundary layers at Mach numbers nominally up to 5 are given in reference 14, although it was reported that air condensation occurred in the base region at the highest Mach number. (A correction was applied for this in the reference paper.)

It was noted in reference 14 that the base pressure measurements obtained did not correlate very well on the basis of the parameters proposed by Chapman, reference 15. However, the test models of reference 14 included ogive cylinders with fineness ratios of 7 and 10, very similar to the fuselage of the present model, and it was assumed that the base pressure data from those models were directly applicable to the present

model at the same Mach number and Reynolds number. Data upon which to base the estimates were therefore interpolated and extrapolated from reference 14 and are shown in figure 7.

The effects of the blunt model tip and the blunt wing leading edge on the base pressure were considered. The thickness of the shear layer produced by the blunt tip of the fuselage was calculated and found to be thin compared to the boundary layer at the base (0.002 inch as compared to 0.012 inch at model scale). Therefore, the properties at the boundary-layer edge were taken to be those of a sharply pointed body, and the base pressure was assumed to be unaffected. The shear layer due to the blunted wing leading edge was also analyzed and found to be unimportant in its effect on the base drag, largely because the bow wave is very weak at high angles of sweepback. The effect was small compared to the estimated uncertainty in the base pressure, and no correction was applied.

Beyond the range of Reller's data (ref. 14), the effect of Reynolds number on the base drag was estimated empirically. The experimentally observed variation of base drag coefficient with Reynolds number was fitted by equations of the form $C_{D_b} = BR^n$, with $n = 0.11$, $B = 5.7/10^4$, for a laminar boundary layer at a Mach number of 4.48 and $n = 0.145$, $B = 4.2/10^4$ for a turbulent boundary layer at the same Mach number. The coefficient B is a function of Mach number which can be obtained from figure 7, but n was assumed independent of Mach number in the range from 4 to 6. At Mach numbers below 4, the value of n for laminar flow increased up to 0.4.

It is believed that the estimates of base drag could easily be in error by 10 percent and might be in error by twice that much.

Discussion of Estimated Minimum Drag

Figure 4(a) shows that, with a laminar boundary layer, the wave drag is the largest part of the total, followed by base drag and skin friction. The wave drag is principally the pressure drag of the leading edge, in spite of the high sweepback angle. Of course, this can be greatly modified by changing the thickness of the leading edge, which on the test model would correspond to a leading edge 4 inches thick at a full-scale length of 50 feet. It is of interest to note that the base drag is by no means negligible even though the Mach number is relatively high. The calculations of reference 1 show that this remains true out to Mach numbers of the order of 12.

In the case of a turbulent boundary layer, the skin friction of the wing panels becomes predominant. The higher skin friction and base drag of the turbulent boundary layer result in the over-all comparison shown in figure 8, where the minimum drag with turbulent boundary layer is

approximately 1.7 times that with a laminar boundary layer. This substantial difference at once shows the extreme desirability of laminar flow for achieving high L/D with this configuration, and also indicates a favorable situation for distinguishing between laminar and turbulent boundary layers by use of total drag measurements.

The estimated variation of minimum drag coefficient with Mach number given in figure 8 was used to correct experimental data to the common nominal Mach number of 6 (appendix B).

Comparison With Estimate and Configuration of Reference 1

Between the estimate of reference 1 and the present estimate, described above, there are differences of two kinds that arise from changes in configuration and from refinements in estimating procedure. Figure 9 shows these differences. The influence of refining the estimating procedure is shown by the comparison of bar A with bar B, both of which are for the model tested. The principal refinements incorporated in A, but not in B, are allowance for body-wing interference in the pressure drag and skin friction, an attempt to allow for detailed variations in base drag with boundary-layer type and Reynolds number (in A), and a small refinement in the calculation of leading-edge pressure drag. The overall result is only slightly different in the case of a laminar boundary layer as a result of compensating changes in the base drag and interference drag, but in the case of a turbulent boundary layer, the refined estimate gives about 8 percent greater drag mainly as a result of the increase in wing panel skin friction.

The differences between the test model and the configuration of reference 1 are shown by comparing A with C, the final estimating procedures being used on both. The significant change in the model was in the thickness of the leading edge, which was 0.020 inch on the test model (required to prevent buckling failure of the wings under the model launching load) as compared to 0.008 inch originally proposed. This causes between A and C a gross reduction in the leading-edge drag and smaller alterations in wing pressure drag and base drag. Thus, the configuration of reference 1 would have, by current estimating procedures, a minimum drag with laminar flow about 18 percent less than the model tested.

RESULTS AND DISCUSSION

The results of this investigation will be discussed under the headings of drag, lift and aerodynamic stability, and lift-drag ratios.

A
2
4
0

Drag

The objectives of the drag measurements were to obtain values of minimum drag and drag due to lift to compare with theory, and to determine the extent of laminar flow as a function of surface roughness. The corrected drag data (appendix B) obtained at a nominal Mach number of 6 and a nominal length Reynolds number of 6 million are plotted in figure 10 as a function of the mean-square angle of attack, which may be regarded as the square of the effective angle of attack. According to equations (A3) and (A8), this presentation should result in a straight line of slope k . The data do, in fact, fall in approximately straight lines with moderate scatter. For comparison, straight lines with slope $k = C_{L\alpha} = 4/\beta$ have been drawn through the theoretical values of C_{D_0} for all-laminar and all-turbulent boundary layers. The lines through the experimental data points were determined by a least squares fit and show steeper slopes than the theoretical lines - 9 percent greater for the smooth models and 19 percent greater for the rough models.

Smooth models.- Figure 10(a) shows the data from the "smooth" model tests. The four classes of surface finish employed did not result in any systematic differences in drag. The smoothest model, represented by the circular data point, did not give indication of the lowest minimum drag (C_{D_0}). The model which did appear to have the lowest minimum drag coefficient had a maximum roughness height of 30 to 35 microinches. The position of this point relative to the others is believed to be fortuitous.

Rough models.- The object of the tests with the rough models was to promote transition to turbulence at the leading edge. The drag data obtained from four models with the surface covered with 100 to 200 microinch scratches approximately normal to the body axis, as in figure 2(a), are shown in figure 10(b). The indicated minimum drag coefficient was only 3 percent greater than that obtained with the smooth models. At small angles of attack, the skin-friction drag was apparently about the same for the smooth and rough models. At large angles of attack, the drag of one roughened model was greater than that of the smooth models and was very close to the predicted turbulent drag curve.

The indication from comparison of the above data with theory is that the boundary layer on the models was partly laminar and partly turbulent, and the shadowgraph pictures gave evidence to the same effect (as will be discussed in a later paragraph). It was therefore believed that rougher surfaces were required to bring about fully turbulent flow. A correlation, given in figure 24 of reference 16, showed that a distributed roughness height of 1600 microinches would be necessary even to start to move transition forward on a body of revolution at this Mach number and

temperature condition. The correlation was largely based on the high-speed data of references 17 and 18, which were from tests with bodies of revolution in the Supersonic Free-Flight Wind Tunnel. Therefore, methods of making the surface considerably rougher were investigated.

Run 493 was made with the sandblasted model shown in figure 2(c). The measured drag from this run is shown by the square on figure 10(c) to be only slightly increased over the data from figure 10(b). Two additional models (runs 537 and 541) were prepared with burrs about 0.002 inch high, distributed along the leading edge, spaced so as to give turbulence over 91 percent of the wetted surface. The spacing was calculated assuming turbulence to originate at each burr and to spread laterally at a 10° angle. The burrs were located 0.3 inch apart and approximately $1/32$ inch back from the leading edge, as in figure 2(a). The drag measurements from these models are shown in figure 10(c) by the diamond and the triangle, and are not significantly different from the data of figure 10(b).

Three models were prepared with similarly spaced burrs 0.006 inch high. A side profile view of one of these burrs is shown in figure 2(d) and a plan view is shown in figure 2(e). The data obtained are marked by the flagged symbols in figure 10(c) and fall within the scatter of the earlier data. No corrections for trip drag have been applied to any of the above data. The trip drag of these last trips is appreciable (approximately 0.001 to 0.0015) if the trips are subject to a mean pressure coefficient of 1 over the frontal area. Applying a correction of this amount would put these points below the earlier drag values. The reason for this strange result is not clear, but it seems probable that the pressure coefficients on the front of the burrs were less than 1, and that the trips, by thickening the boundary layer, lowered the skin friction somewhat, thereby compensating in part for the trip drag.

Three remaining test models had notches filed in the wing leading edge every 0.1 inch. The notch depths were between 0.0055 inch and 0.0074 inch (see fig. 2(f)). The drag coefficients of these models are shown in figure 10(d). At low angles of attack, the data (uncorrected for trip drag) fell very near the theoretical turbulent drag line. At high angles of attack, the data from one model fell above this line. Estimates of the trip pressure drag were in this case very uncertain because of the complicated flow in the vicinity of a notch, and it was concluded that no quantitative interpretation of these measurements could be made.

Comparison with reference 2.- In figure 10(e) the data from the smooth models are compared with the wind-tunnel data of reference 2. The data of reference 2 have been adjusted to correspond to the reference area employed in the present test. The minimum drag coefficient from the wind-tunnel test is 48 percent above the minimum drag of the present smooth models. Furthermore, the wind-tunnel data are foredrag data; the base drag is yet to be added. The factors which are available to account for the difference in C_{D_0} are a difference in Reynolds number, 1 million

compared to 6 million, and differences in configuration. The principal difference in configuration was in body fineness ratio, 7.0 in the wind-tunnel model compared with 9.5 in the present models. Effectively, this makes the body cross-sectional area 84.3 percent greater (for the same wing area) in the case of the wind-tunnel model.

A series of approximate adjustments was applied to the wind-tunnel data to see if it would be brought into closer alignment with the present results by appropriate changes in Reynolds number and body cross section. The body pressure drag and skin friction were reduced to "shrink" the body by use of the estimation procedures described earlier, and the total skin friction was adjusted to account for a change in Reynolds number from 1 million to 6 million. These adjustments were estimated for the cases of all-laminar boundary layer and all-turbulent boundary layer. A small adjustment to leading-edge drag was required to make the leading-edge diameters comparable. The base drag estimated for the test Mach number and Reynolds number was then added to convert the foredrag to total drag. These adjustments resulted in the values of C_{D_0} indicated by the ticks shown on the drag-coefficient axis in figure 10(e), the upper one corresponding to adjustments based on turbulent boundary layer, the lower one, laminar boundary layer. These adjusted values are within about 25 percent of the present experimental results and show a minimum drag close to the theoretical value for a turbulent boundary layer.

A
2
4
0

It should also be noted that the slope of the drag curve from the wind-tunnel tests is somewhat greater than that from the present tests. This is consistent with the fact that the wind-tunnel lift coefficients were somewhat greater than those obtained from the present test, as will be discussed in a later paragraph.

Correlation of minimum drag measurements with shadowgraph pictures.-

The boundary layer coming off the base of the test models frequently can be detected in the shadowgraph pictures. A background of turbulence in the wind-tunnel boundary layer on the windows is also present and tends to obscure the model boundary layer, but the model turbulence, being from a very thin boundary layer, is finer grained and closer spaced than the wind-tunnel wall turbulence. Furthermore, regions of laminar and turbulent flow in the model wake sometimes occur in close proximity to one another, and then the contrast is very evident. This is the case in figure 3(a) where a transition front appears in the wake. This front is inclined relative to the free stream but is not quite parallel to the model leading edge. It crosses the wing base at about 0.3 to 0.4 inch from the tip, which implies a transition Reynolds number of 2.0 to 2.5 million at the point of crossing. If the transition Reynolds number is assumed constant across the span, 1/3 to 1/2 of the model surface is in turbulent boundary-layer flow.

Another interesting feature of the pictures (fig. 3(a)) is the appearance of a series of streamwise streaks in the laminar regions

behind the wing tips. These streaks begin some distance behind the base and terminate in turbulence. It is believed that these streaks are related to similar streaks found by numerous investigators by means of evaporative surface coatings. They are usually said to be streamwise vortices. Such markings have almost invariably been reported from investigations of sweptback wings. A thorough study which reported the streaks and attributed them to vortex development on swept wings and spinning disks was published in reference 19.

With the basic rough models, the distance in from the wing tip over which laminar flow regions in the wake could be observed was reduced to less than 0.2 inch typically (fig. 3(b)). Also the flow in this region was intermittently turbulent. Addition of the sandblasted strip or the 0.002-inch burrs along the leading edge gave pictures, such as figures 3(c) and 3(d) which appeared to show essentially an all turbulent boundary layer (except possibly for a narrow strip near the leading edge), but some pictures of the model with the 0.002-inch burrs indicated that the flow in the tip region may have again been intermittently laminar. With the 0.006-inch burrs, turbulent flow appeared to have been obtained over most of the model (fig. 3(e)). Waves due to these burrs can be seen in this figure between the lower wing panels and the bow shock wave.

A similar view of a model with a notched leading edge is given in figure 3(f). The trip waves are in this case closer spaced, because the notches were only 0.1 inch apart, and also appear to be weaker than the burr waves. This trip was evidently successful in producing a turbulent boundary layer over the entire surface. The turbulence associated with the upper two wing panels is very conspicuous. Although the angle of attack in this picture is rather high, pictures at lower angles showed essentially similar features.

The last picture (fig. 3(g)) shows a rough-surfaced model at approximately double the Reynolds number of the preceding pictures. In this case the boundary layer coming off the base is very definitely turbulent with the possible exception of a very narrow region (0.030 inch wide, spanwise) near the wing tips.

Tests at higher Reynolds number.- A few additional models were tested at Reynolds numbers in the range from 11 million to 16 million. The results obtained are shown in a plot of C_{D_0} as a function of Reynolds number in figures 11(a) (smooth models) and 11(b) (rough models); C_{D_0} was obtained from the measured C_D by use of the experimental drag due to lift shown in the preceding figure. Points for values of α_r^2 greater than 0.008 were eliminated because of possible uncertainty in the correction. The data show a relative insensitivity of C_{D_0} to Reynolds number in this range. The data for the rough models appear to indicate a slight increase in C_{D_0} with increasing Reynolds number, while those for the

smooth models appear to indicate a small decrease in drag, about what would be obtained at a constant relative position between the theoretical curves. This gives the smooth models an advantage in minimum drag of about 10 percent at a Reynolds number of 12 million, as compared to an advantage of 3 percent at the lower Reynolds numbers. The shadowgraph pictures showed essentially all-turbulent wakes from both the smooth and rough models. It is possible that the observed difference between the drag coefficients of the smooth and rough models at high Reynolds number is due to an increase in the turbulent skin friction with increased surface roughness.

Discussion.- Of the various roughened models, perhaps the most successful were those with the sandblasted strip and with the 0.002-inch burrs, both of which appeared to give a substantially all-turbulent boundary layer without large amounts of trip drag. The minimum drag of these models (fig. 10(c)) is less than the theoretical estimate for turbulent boundary layer by about 10 percent. If it is assumed that a 0.1-inch strip along the leading edge remained laminar, the underestimate becomes 7.5 percent. Although it was not certain that the boundary layer on these models was entirely turbulent, the fact that the minimum drag appears to have converged to a limiting value not exceeded with any of the larger trips strongly suggests that, for practical purposes, turbulent flow was realized. The shadowgraph pictures substantiate this belief.

It is interesting to note that the total-drag estimate of reference 1 for a turbulent boundary layer agreed with the measured value within 2.5 percent. If the error in the present estimate is all ascribed to the estimate of skin friction, it amounts to a 25-percent error in the estimated skin friction and corresponds approximately to the increase in skin friction calculated to result from body-wing interference. Whether this correspondence is significant or not cannot be stated.

It is noteworthy that the difference in minimum drag between the smooth models and the rough models with all-turbulent boundary layer was small compared to the expected difference between models with all-laminar and all-turbulent boundary layers. It can be speculated that at Reynolds numbers below 3 million, a closer approach to the all-laminar drag might occur.

No evaluation of the laminar flow estimates can be directly made, since fully laminar flow was never obtained or approached. However, the drag of the smooth models can be tested for consistency with the laminar theory in the following way: For an assumed transition front parallel to the leading edge, a theoretical variation of the skin-friction drag of a triangular wing as a function of streamwise distance to transition can be calculated, with an allowance for starting length of the turbulent region as employed in reference 12. The results of such a calculation are given in figure 12, in terms of the fractional distance between the laminar and turbulent skin-friction curves as a function of transition

location. For comparison, the curve obtained from a simple ratio of the area covered with a turbulent boundary layer to the total wetted area is shown and is a fairly good approximation to the more exact curve. The shadowgraph pictures of the smooth models suggest a value of $5/12$ for x_t/l - hence, the skin friction of the wings should be the laminar value plus 0.38 of the difference between the laminar and turbulent values. This fraction, although derived for the wings alone, was applied to the total skin friction. The base drag was also estimated on the basis of a turbulent boundary layer inboard and a laminar boundary layer over the wing tips. The estimated minimum drag coefficient for the smooth models thus obtained was 0.0100 compared to the experimental value of 0.01095 , an underestimate of 9.5 percent. These considerations show that the smooth-model data with a transition Reynolds number of 2.5×10^6 are in reasonable alignment with the theoretical estimates.

The fact that the drag due to lift of the rough models was somewhat greater than that for the smooth models is of some interest. The cause is speculative. It should be noted that this indication is based entirely on the results from run 181, and may have been due to experimental error. On the other hand, it may have been another indication of an increase in skin friction due to surface roughness, since the boundary layers are thinned on the windward side of the model at angle of attack.

Lift and Aerodynamic Stability

Seventeen test runs were selected for analysis of lift and aerodynamic stability by the machine-programmed method described in appendix A. Of the seventeen, results were obtained from twelve, with the process failing to converge for the other five. It was noted that the five models for which the analysis did not converge had relatively high roll rates, all over 5° per foot (over 2500 rpm). However, two of the successful runs had roll rates of 6.26° and 6.43° per foot. Another point of difference lies in the eccentricity of the elliptical figures of the angular motion in the $\alpha - \beta$ plane. The ratio of the minor axis to the major axis was computed, and the five models which could not be analyzed had ratios ranging from 0.4 to 0.7 , whereas the twelve successful runs ranged from 0.03 to 0.3 .

Table II shows the root-mean-square variation in the fit of the theoretical motion curves to the data. When the fitted curves for α and β have rms errors within 0.07° , they are within the reading error. Likewise, rms errors in y and z , which are less than 0.005 inch, are within the reading error. In figures 13(a) and (b), data points from one of the better runs, run 493, have been plotted along with the fitted curves. The closeness of the experimental points to the computed curves are a measure of the reliability of the lift and stability results.

Lift curve slope.- The measured values of lift-curve slope are shown in figure 14 in the form $\beta C_{L\alpha}$ as a function of $\beta \cot \Lambda$. The estimate of the lift curve slope shown on this figure is based on the expectation that the lift of the two wing panels might be comparable to the lift of a plane triangular wing with a span equal to the straight-line distance between the wing tips. Figure 14 shows that the lift realized at the test Mach number is within about 10 percent of the linearized theoretical lift of the plane triangular wing. An isolated test point was obtained at the considerably lower test Mach number of 4.4, and it indicates an appreciable drop in $\beta C_{L\alpha}$ as the Mach cone angle approaches the sweep angle. For comparison, results of tests of the modified configuration from reference 2 are included. These data are in reasonable alignment with the present data except for the test point from reference 2 at $M = 6.28$ which is about 20 percent higher. These data indicate an increase in lift developed relative to linearized theory as the Mach number is increased, and in this respect are in agreement with data for planar wings (see, e.g., ref. 20).

A
2
4
0

To investigate the presence of nonlinearities in the lift curve, the data of figure 14 were plotted as a function of pitching amplitude in figure 15. If the lift curve is assumed to be linear in the small angle range, the two points available at angles of attack of 8° and 10° indicate that the lift coefficients may, in this range, be less than the linear values. (It is equally possible that these two points are on the lower edge of the scatter band, although it is noted that these two values were the lowest obtained.) This trend is in contrast to the estimate in reference 1 of a lift curve with a linear term and a Newtonian quadratic term

$$C_L = (4/\beta)\alpha + 2\alpha^2 \quad (2)$$

The values of $\beta \bar{C}_{L\alpha}$ (where the bar denotes an average value) which would be measured by the present linear, data-reduction technique from the lift curve given by equation (2) have been estimated and included on figure 15. The Newtonian contribution to the lift is plainly not realized.

The data of reference 2 for the modified three-wing configuration are included on the figure, and show the presence of some favorable nonlinearity at Mach numbers from 4 to 5. It is far short of the Newtonian nonlinearity. The Mach number 6.28 data show a characteristic somewhat similar to the present data although at a somewhat higher level. It is possible that this high level of the $M = 6.28$ data is due to experimental error in defining the initial slope. However, as pointed out earlier, the drag rise curve at this Mach number also had a steeper-than-expected slope, supporting the lift measurements.

Concerning the nonlinearity in the case of plane wings, the data of reference 20 show that it is considerably short of that given by equation (2). A coefficient of the α^2 term of 0.5 or less is much more realistic than a coefficient of 2 in the angle-of-attack range considered here, and, in fact, a cubic nonlinearity fits the data better than a quadratic. Hence, on the basis of these three tests, equation (2) is not recommended for estimation of the nonlinear lift in the small-angle range.

Static stability.- The stability data obtained are shown in figure 16, where $C_{m\alpha}$ is plotted as a function of center-of-gravity position.

A
2
4
0
In the analysis of data (appendix A), the model is assumed to be aerodynamically symmetric, so that while the symbol $C_{m\alpha}$ appropriate to the pitch plane is used, it is understood that this represents the average stability of the model in all roll attitudes, and that the models were actually rolling very fast during the test. The square symbols represent results of another method of analysis in which the model pitch plane and yaw planes are identified and allowed to take different values of the stability derivative. This type of analysis did not show any differences in the static stability in pitch and sideslip within the scatter of the data, so these data also are averaged for presentation in figure 16. However, since the scatter is appreciable, a 10- or 20-percent difference could exist without being defined.

The data have been corrected to a common Mach number of 6 by use of the relation

$$C_{m\alpha_{\text{corr}}} = C_{m\alpha} \left(C_{N\alpha, M=6} / C_{N\alpha} \right) \quad (3)$$

which assumes that the center of pressure does not vary with Mach number over the range of the correction. Equation (A20) was used to obtain a value for $C_{N\alpha}$, and C_D , which is small compared to $4/\beta$, was given the constant value of 0.013; $C_{N\alpha, M=6}$ is then 0.689.

The slope of the data in figure 16 is the experimental value of $C_{N\alpha}$ and the intercept on the center-of-gravity axis is the center of pressure. A line fitted to the data by least squares is shown, and it indicates a normal-force-curve slope of 0.746 and a center of pressure at 64.3-percent length. (Note that the center-of-gravity and center-of-pressure positions are measured from the position of the sharp tip, before blunting.) The experimental normal-force-curve slope minus the mean drag coefficient, 0.013, gives a second value for the lift-curve slope, 0.733, or $\beta C_{L\alpha} = 4.34$, which is 12-1/2 percent higher than the value obtained

from the swerve data. If the normal-force-curve slope is taken from the swerve lift data, $C_{N_\alpha} = 0.664$, and a line of this slope is fitted to the C_{m_α} data (dashed line on fig. 16), the center of pressure is at 65.1-percent length.

The expected location of the center of pressure, from the simplified viewpoint of reference 1, was at 66.7-percent length, which is the centroid of plan-form area. The presence of body lift, which is largely concentrated on the body nose, will tend to move the center of pressure forward. Evidently, the forward movement was not appreciable. The center-of-pressure location found in reference 2 at this Mach number was at 67.6-percent length.

Dynamic stability.— As a by-product of the static-stability reduction, values of the damping parameter, ξ , were obtained and are shown in figure 17. The definition of this parameter was not too good, and no concentrated effort was made to determine the causes of the scatter or to reduce it. It was observed that plotting against amplitude of oscillation did not reduce the scatter as it could be expected to do if the cause of the scatter were nonlinearity of the damping with angle of attack.

Damped motions were observed in every case, as evidenced by the negative values of the coefficient ξ . For the case of nonrolling flight at constant altitude, the significance of ξ can be identified from the following equation:

$$\alpha_m/\alpha_{m_1} = e^{\frac{\rho A}{4m} \xi x} \quad (4)$$

The data were reduced through equation (A17) to the form $C_{m_q} + C_{m_\alpha}$ and were compared with the simple results of slender body theory given in reference 21. The average of the measured coefficients appeared to be about half of the theoretical value.

Lift-Drag Ratios

The aerodynamic efficiency of the test configuration can now be estimated from experimental values of the lift and drag coefficients. A number of different flight conditions can be visualized for this purpose in which the Reynolds number and leading-edge thickness are varied over some realistic range. Aerodynamic heating dictates the use of a large diameter leading edge, while aerodynamic efficiency requires a thin leading edge. The leading edge employed in the tests corresponds, for a scale factor of 200, to a 4-inch diameter at full scale. The leading edge assumed in reference 1 was 1.5 inches in diameter.

The leading-edge heating considerations given in reference 1 indicate that the heating can easily become critical. The estimated radiation equilibrium temperature of the 1.5-inch diameter leading edge ranged from 1700° F at a Mach number of 6 to 3200° F at a Mach number of 12 for emissivity = 0.6. It can be quickly estimated that the 4-inch leading edge would have corresponding temperatures at a Mach number of 12 of 2800° F for an emissivity of 0.6 and 2600° F for an emissivity of 0.9. Thus, the temperature reductions due to increasing the leading-edge diameter and the emissivity are not large, but may nevertheless be essential since the working limits of available leading-edge materials fall into this same range.

A
2
4
0

It will therefore be assumed, in the following, that the 4-inch leading edge represents the large diameter that may be required because of heating; and that the 1.5-inch leading edge represents the optimistically small diameter that might possibly be satisfactory in the Mach number range below 12. The following table then gives the minimum drag coefficients for these two leading edges at Reynolds numbers of 6 million and 14.6 million (equilibrium glide Reynolds number for Mach number of 6 from ref. 1) for the smooth and rough models.

R	Test models, experiment		Experiment adjusted to $d_{le} = 1.5$ in.		Estimated, ref. 1	
	Smooth	Rough	Smooth	Rough	Laminar	Turbulent
6.0×10^6	0.01095	0.01125	0.00954	0.00984		
14.6×10^6	.01025	.01155	.00884	.01014	0.0062	0.0097

The method of adjusting the minimum drag for the change in leading-edge diameter is the one described under estimation of minimum drag coefficient.

The estimated L/D will differ from experiment because of the above differences between estimated and measured minimum drag and also because of error in the estimated lift coefficient. At an angle of attack of 0.1 radian, which is near the angle for maximum L/D, the experiment indicates a lift coefficient of 0.0643, while the estimated value was 0.0876. The discrepancy is 90 percent due to the assumption of a Newtonian nonlinear term in the lift equation, and 10 percent due to an error in initial slope. The discrepancy in lift coefficient, which affects also the drag due to lift, is by far the most serious discrepancy in the estimates of reference 1.

Now, by use of the above-tabulated values of C_{D_0} and the experimental lift values indicated by the solid line through the data in figure 15, together with the experimentally indicated drag due to lift shown in figure 10(a), the values of lift-drag ratio shown in figure 18 were obtained. Curve I is the smooth test model at the test Reynolds number

of 6 million. Curve II is the smooth test model at a Reynolds number of 14.6 million. Curve III is the adjusted experimental L/D curve for a smooth model with a leading-edge diameter equivalent to 1.5 inches at full scale. Curve IV is the original theoretical estimate of reference 1. Also included for comparison is the experimental data of reference 2, presented without modification, for a Mach number of 6.28 and a Reynolds number of 1 million.

The turbulent boundary-layer curve from reference 1 was used for comparison in figure 18 because it was indicated that the boundary layer of the smooth models was appreciably turbulent at the lower Reynolds numbers and essentially all-turbulent at the higher Reynolds numbers. The failure of the model to attain the theoretical L/D is due largely to the overestimate of lift discussed above, and secondarily, to a slightly higher than theoretical development of drag due to lift. It appears that a maximum lift-drag ratio of about 4.0 (including base drag) is the limit of performance of the configuration at this Mach number and for the range of test Reynolds numbers.

CONCLUDING REMARKS

The above program to investigate the aerodynamic characteristics of a highly swept three-wing hypersonic glider configuration, at a Mach number of 6 and Reynolds numbers from 6 to 16 million, has led to the following conclusions. These conclusions, of course, will not necessarily apply to other hypersonic glider configurations, but may be indicative of some general characteristics of such vehicles.

1. At a length Reynolds number of 6 million, the transition Reynolds number on the smooth models was estimated from the shadowgraph pictures to be about 2.5 million. The minimum drag measurements were consistent with this estimate.

2. Varying the surface smoothness from highly polished to roughened did not appreciably influence the minimum drag although it did cause small changes in the regions over which the wake was turbulent. This indicates that surface roughness played a minor role in determining the transition point over the range of roughnesses covered.

3. Changing the Reynolds number from 6 to 16 million caused only small changes in the experimental minimum drag for both smooth and roughened models. An effect of surface roughness on turbulent skin friction was apparently detected in the case of the roughened models.

4. The methods used to estimate the minimum drag in reference 1 and the present report were found to be accurate within about 10 percent, the estimates of reference 1 being somewhat more accurate than the present, more detailed methods.

5. The drag due to lift was underestimated by about 10 percent for the smooth models by use of the standard relation, $C_D - C_{D_0} = C_L \alpha$. For the rough models, the values of drag due to lift were still higher, possibly as a result of roughness effect on skin friction on the windward side of the models at angle of attack.

6. The estimate of the initial lift-curve slope by linearized plane triangular wing theory was accurate within 5 percent, although this close agreement was somewhat fortuitous. The available data indicate that poorer agreement would be obtained at both higher and lower Mach numbers.

A
2
4
0
7. The Newtonian nonlinearity incorporated in the lift estimates of reference 1 was not realized. The lift curves were essentially linear in the range up to 10° .

8. The static stability was given with satisfactory accuracy by the above lift information and a center of pressure at the centroid of plan-form area. The presence of body lift moved the center of pressure forward by less than 2 percent of the length from this location.

9. The expected axial symmetry of the static stability was apparently realized, although the tests could not be used to detect small changes in stability with roll orientation.

10. The configuration was dynamically stable.

11. The lift-to-drag ratios were appreciably below the estimated values of reference 1, largely because the Newtonian nonlinearity in lift was not realized experimentally. The lift-drag ratio of the smooth model (which had a significant amount of turbulent boundary layer) was 4.0, 19 percent below the value expected with all-turbulent boundary layer.

Ames Research Center
National Aeronautics and Space Administration
Moffett Field, Calif., July 26, 1960

APPENDIX A

REDUCTION OF DATA

DRAG

The reduction of drag coefficient from the time-distance data was based on the procedure described in reference 22, the basic equation being

$$d(\ln V)/dx = -KC_D \quad (A1)$$

where $K = \rho A/2m$. To a very good order of approximation for the small variation in velocity characteristic of these models, the plot of V against x will be linear, in accordance with the approximate equation

$$C_D = -(dV/dx)/K\bar{V} \quad (A2)$$

where dV/dx is the mean slope of the slightly curved line and \bar{V} is the mean velocity in the test section. A plot of velocity against distance is given in figure 19 and illustrates the definition of the slope, dV/dx , that was obtained from a run with very small angles of attack and excellent time and distance data. The velocity loss in the test section was of the order of 0.5 percent. Distance errors of 0.005 inch or time errors of 0.09 microsecond will give velocity errors of 0.5 ft/sec. Runs in which the raw data were not of suitable accuracy (e.g., because of double-exposed pictures) were discarded.

For runs with larger amplitudes of pitching oscillation, it was necessary to consider the variation in drag with angle of attack. The models usually underwent about 1-1/2 cycles of oscillation in the test section, and their total drag doubled when the angle of attack was changed from 0° to between 7° and 8° . The tests included angles of attack as high as 11.1° . Therefore considerable departure from the constant drag force assumed in derivation of equations (A1) and (A2) occurred. (A variation in C_D with x is always encountered in ballistics range testing, but the variation is rarely as large as it was here.) For illustration, the velocity curve that was obtained from run 181 is reproduced in figure 20, along with the variation in resultant angle of attack. In this run the scatter of the velocities from the single (3-foot) intervals was small enough that an oscillation of the velocity curve corresponding to the oscillation in resultant angle of attack can be observed. The slope of the velocity curve is maximum when α_r is maximum, and vice versa. The variation in local slopes is of the order of 2/1. However, the local drag cannot be accurately obtained from the local slope because the accuracy

of the time-distance data is not sufficient to define the local slope. Therefore, it was necessary to determine how this kind of a run could be analyzed with some degree of exactness. The analysis that was made is reproduced below.

The drag coefficient is assumed to vary with the square of the local resultant angle of attack according to the relation

$$C_D = C_{D_0} + k\alpha_r^2 \quad (A3)$$

(The constant k is normally taken to be the lift-curve slope.) Then,

$$\left(C_{D_0} + k\alpha_r^2\right) \frac{1}{2} \rho V^2 A = -mV \frac{dV}{dx} \quad (A4)$$

or

$$K \left(C_{D_0} + k\alpha_r^2\right) dx = -\frac{dV}{V} \quad (A5)$$

Integrating from $x = 0, V = V_i$ to x, V gives

$$K \left(C_{D_0} x + k \int_0^x \alpha_r^2 dx\right) = -\ln \frac{V}{V_i} \quad (A6)$$

The quantity in parenthesis replaces the product $C_D x$ found in the equation for constant drag coefficient. Hence the quantity in parenthesis is the product of the effective drag coefficient $C_{D_{eff}}$ and the distance x , that is

$$C_{D_{eff}} x = C_{D_0} x + k \int_0^x \alpha_r^2 dx \quad (A7)$$

$$C_{D_{eff}} = C_{D_0} + k \frac{\int_0^x \alpha_r^2 dx}{x} = C_{D_0} + k \overline{\alpha_r^2} \quad (A8)$$

Hence the effective drag coefficient is the drag coefficient that would be obtained at a resultant angle of attack equal to the root mean square resultant angle of attack, averaged over the distance interval x . It should be noted (eq. (A6)) that only the end point velocities, V and V_i , enter into this result.

For cases where the pitching moment is linear, and the oscillations of the model are uncoupled, and undamped,

$$\alpha_r^2 = \alpha_m^2 \sin^2 2\pi \frac{x + x_\alpha}{\lambda} + \beta_m^2 \sin^2 2\pi \frac{x + x_\beta}{\lambda} \quad (A9)$$

and the integral in equation (A6) can be evaluated to yield

$$\begin{aligned} -\ln \frac{V}{V_i} = & K \left(C_{D_0} + k \frac{\alpha_m^2 + \beta_m^2}{2} \right) x \\ & - \frac{K\lambda}{8\pi} k \left(\alpha_m^2 \sin 4\pi \frac{x + x_\alpha}{\lambda} + \beta_m^2 \sin 4\pi \frac{x + x_\beta}{\lambda} \right) \\ & + \frac{K\lambda}{8\pi} k \left(\alpha_m^2 \sin 4\pi \frac{x_\alpha}{\lambda} + \beta_m^2 \sin 4\pi \frac{x_\beta}{\lambda} \right) \end{aligned} \quad (A10)$$

A
2
4
0

The right-hand side of equation (A10) has a term linear in x , a periodic term with a frequency twice the pitching frequency and a constant term which depends on the initial phase of the α and β oscillations. Physically, the first two terms represent the equation of the mean line of velocity versus distance and the fluctuations about the mean line, respectively. Hence, the equation of the mean line is

$$-\ln \frac{V}{V_i} = K \left(C_{D_0} + k \frac{\alpha_m^2 + \beta_m^2}{2} \right) x = KC_{D_{\text{eff}}} x \quad (A11)$$

where $C_{D_{\text{eff}}}$ is the drag coefficient given by the slope of the mean line, and the effective angle of attack squared is

$$\overline{\alpha_r^2} = \frac{\alpha_m^2 + \beta_m^2}{2} \quad (A12)$$

These equations permit the analysis of a run like run 181 from the slope of the mean line of velocity versus distance. The mean line has been drawn in figure 20, and is curved. There is a corresponding diminution of $(\alpha_m^2 + \beta_m^2)$ during the course of the flight. Because of this, it was possible to obtain values of C_D at α_r ranging from 5.4° to 7.5° from run 181, and similar multiple values of C_D from other large angle flights.

Frequently the pitching and yawing motions were roll-coupled and equation (A12) could not be used. (This could be determined by plotting the motion in the $\alpha - \beta$ plane where deviations from simple harmonic motion are easily detected.) In such cases graphical integration was employed to determine α_r^2 for use in equation (A8). The requirement

of equation (A8) for local velocities at the beginning and end points of the distance interval over which C_D is being determined was met by choosing these intervals between points of minimum and maximum α_r . At such points the oscillating velocity curve crosses the mean line. Hence, the problem reduces to determining experimentally the mean line of velocity versus distance. This is accomplished by using only the relatively long two- and three-station intervals in the calculation of points for the velocity curve. Comparison of results obtained by use of this procedure and the analytical procedure described in the preceding paragraph in the case of run 181 gave excellent agreement.

These procedures are believed to account in a precise way for the variations of drag of a pitching model in a ballistic range.

STABILITY AND LIFT

If the motion of a vehicle in flight can be described by equations relating the angle of attack and the swerving motion to distance (or to time), the stability and lift coefficients can be determined - the static stability from the pitching frequency, the dynamic stability from the rate of change of pitch amplitude, and the lift coefficient from the swerving motion. The method involves the fitting of equations of motion to the data obtained, where the constants to be adjusted in obtaining the fit are the aerodynamic coefficients and the initial conditions of the motion. This is the usual procedure for ballistic ranges. In the present case, the machine computation method described in reference 23 was employed to select the best fitting coefficients by an iterative process. If the process converges as in the example shown in figure 13, values are obtained, the adequacy of which is determined by the resultant fit. If the process diverges, no results are obtained.

Stability coefficients were obtained using the equations of motion (including the effects of trim and roll) given in reference 24, namely,

$$\beta + i\alpha = K_1 e^{(\eta_1 + i\omega_1)x} + K_2 e^{(\eta_2 - i\omega_2)x} + K_3 e^{ipx} \quad (A13)$$

$$\eta_1 + \eta_2 = \frac{\rho A}{2m} \xi \quad (A14)$$

$$\frac{2\pi}{\sqrt{\omega_1 \omega_2}} = \lambda \quad (A15)$$

$$C_{m\alpha} = - \frac{8\pi^2 I_y}{\lambda^2 \rho A l} \quad (A16)$$

The dynamic stability parameter, ξ , was computed from equation (A14). The damping-in-pitch derivative, $C_{m\dot{q}} + C_{m\dot{\alpha}}$, was computed from the relation,

$$\xi = C_D - C_{L\alpha} + (C_{m\dot{q}} + C_{m\dot{\alpha}}) \left(\frac{l}{\sigma}\right)^2 \quad (\text{A17})$$

The static-stability derivative, $C_{m\alpha}$, was computed from equation (A16).

The lift curve slope was obtained from the solution of the differential equation for the swerving motion (ref. 24) which was adapted for machine computation employing a least squares fit. The working equation is

$$\begin{aligned} -y + iz = (-y + iz)_i + (-y + iz)'_i x + 12 \frac{\rho A}{2m} \left[C_{L\alpha} \int_0^x \int_0^x (\beta + i\alpha) dx dx \right. \\ \left. + (-C_{Y_0} + iC_{L_0}) \left(\frac{1 + ipx - e^{ipx}}{p^2} \right) \right] \quad (\text{A18}) \end{aligned}$$

The center-of-pressure position was found from the relation

$$C_{m\alpha} = C_{N\alpha} \left(\frac{x_{cg} - x_{cp}}{l} \right) \quad (\text{A19})$$

where

$$C_{N\alpha} = C_{L\alpha} + C_D \quad (\text{A20})$$

in the small angle range.

APPENDIX B

CORRECTIONS TO MEASURED DRAG COEFFICIENTS

Twenty-two models were employed in the measurement of drag, and since these models were not all geometrically identical and since they departed slightly from the nominal test conditions, small corrections were applied to bring the measured points to standard test conditions and standard geometry. The uncorrected data and the corrections are given in table I. The total of all corrections was less than 5 percent except in three cases which ranged from 6.3 to 9.9 percent, as indicated in table I.

The corrections were applied for deviations in Mach number and Reynolds number from 6.0 and 6.0 million, respectively, and for deviations in leading-edge thickness, tip bluntness, and base area, etc., from standard dimensions. The corrections were computed for $\alpha = 0$ on the assumption that the increment in C_{D_0} would not affect the drag due to lift. The leading-edge thickness correction was ordinarily the largest and was calculated by the method outlined under the section on drag estimation. The correction to the base drag for deviations in base area, Mach number, and Reynolds number was, for the case of the smooth models, based on the assumption that the body base and inboard one-third of the wing base were in a turbulent boundary-layer region and the outboard two-thirds of the wing panel was in a laminar boundary-layer region. The boundary layers of the roughened models were assumed to be fully turbulent. These assumptions are not critical, however, because of the small size of the corrections. The correction to the skin-friction drag for departures in Mach number and Reynolds number from standard test values was made by requiring that the relative position of the uncorrected data point between the theoretical laminar and turbulent skin-friction curves remain unchanged.

REFERENCES

1. Seiff, Alvin, and Allen, H. Julian: Some Aspects of the Design of Hypersonic Boost-Glide Aircraft. NACA RM A55E26, 1955.
2. Savin, Raymond C., and Wong, Thomas J.: Lift, Drag, and Static Longitudinal Stability Characteristics of Configurations Consisting of Three Triangular Wing Panels and a Body of Equal Length at Mach Numbers From 3.00 to 6.28. NACA RM A55K21, 1956.
3. James, Carlton S.: Aerodynamic Performance and Static Stability at Mach Number 3.3 of an Airplane Configuration Employing Three Triangular Wing Panels and a Body of Equal Length. NASA TN D-330, 1960.
4. Delany, Noel K.: Exploratory Investigation of the Low-Speed Static Stability of a Configuration Employing Three Identical Triangular Wing Panels and a Body of Equal Length. NACA RM A55C28, 1955.
5. Delany, Noel K.: Additional Measurements of the Low-Speed Static Stability of a Configuration Employing Three Triangular Wing Panels and a Body of Equal Length. NACA RM A55F02a, 1955.
6. Seiff, Alvin: A Free-Flight Wind Tunnel for Aerodynamic Testing at Hypersonic Speeds. NACA Rep. 1222, 1955.
7. Wilkins, Max E., and Darsow, John F.: Finishing and Inspection of Model Surfaces for Boundary-Layer-Transition Tests. NASA MEMO 1-19-59A, 1959.
8. Penland, Jim A.: Aerodynamic Characteristics of a Circular Cylinder at Mach Number of 6.86 and Angles of Attack Up to 90°. NACA TN 3861, 1957.
9. Ehret, Dorris M., Rossow, Vernon J., and Stevens, Victor I.: An Analysis of the Applicability of the Hypersonic Similarity Law to the Study of Flow About Bodies of Revolution at Zero Angle of Attack. NACA TN 2250, 1950.
10. Rossow, Vernon J.: Applicability of the Hypersonic Similarity Rule to Pressure Distributions Which Include the Effects of Rotation for Bodies of Revolution at Zero Angle of Attack. NACA TN 2399, 1951.
11. Van Driest, E. R.: Investigation of Laminar Boundary Layer in Compressible Fluids Using the Crocco Method. NACA TN 2597, 1952.
12. Sommer, Simon C., and Short, Barbara J.: Free-Flight Measurements of Turbulent-Boundary-Layer Skin Friction in the Presence of Severe Aerodynamic Heating at Mach Numbers From 2.8 to 7.0. NACA TN 3391, 1955.

- A
2
4
0
13. Maloney, Joseph P.: Drag and Heat Transfer on a Parabolic Body of Revolution (NACA RM-10) in Free Flight to a Mach Number 2 with Both Constant and Varying Reynolds Number and Heating Effects on Turbulent Skin Friction. NACA RM L54D06, 1954.
 14. Reller, John O., Jr., and Hamaker, Frank M.: An Experimental Investigation of the Base Pressure Characteristics of Nonlifting Bodies of Revolution at Mach Numbers From 2.73 to 4.98. NACA TN 3393, 1955.
 15. Chapman, Dean R.: An Analysis of Base Pressure at Supersonic Velocities and Comparison with Experiment. NACA Rep. 1031, 1951.
 16. Seiff, Alvin, Sommer, Simon C., and Canning, Thomas N.: Some Experiments at High Supersonic Speeds on the Aerodynamic and Boundary-Layer Transition Characteristics of High-Drag Bodies of Revolution. NACA RM A56I05, 1957.
 17. Carros, Robert J.: Effect of Mach Number on Boundary Layer Transition in the Presence of Pressure Rise and Surface Roughness on an Ogive-Cylinder Body with Cold Wall Conditions. NACA RM A56B15, 1956.
 18. James, Carlton S.: Boundary-Layer Transition on Hollow Cylinders in Supersonic Free Flight as Affected by Mach Number and a Screwthread Type of Surface Roughness. NASA MEMO 1-20-59A, 1959.
 19. Gregory, N., Stuart, J. T., and Walker, W. S.: On the Stability of Three-Dimensional Boundary Layers with Application to the Flow Due to a Rotating Disk. Phil. Trans. Roy. Soc. (London), Ser. A, vol. 248, no. 943, July 14, 1955, pp. 155-199.
 20. Bertram, Mitchel H., and McCauley, William D.: An Investigation of the Aerodynamic Characteristics of Thin Delta Wings with a Symmetrical Double-Wedge Section at a Mach Number of 6.9. NACA RM L55B14, 1955.
 21. Sacks, Alvin H.: Aerodynamic Forces, Moments, and Stability Derivatives for Slender Bodies of General Cross Section. NACA TN 3283, 1954.
 22. Seiff, Alvin: A New Method for Computing Drag Coefficients from Ballistic Range Data. Jour. Aero. Sci., vol. 25, no. 2, Feb., 1958, pp. 133-134.
 23. Sommer, Simon C., Short, Barbara J., and Compton, Dale L.: Free-Flight Measurements of Static and Dynamic Stability of Models of the Project Mercury Re-entry Capsule at Mach Numbers 3 and 9.5. NASA TM X-373, 1960.
 24. Nicolaidis, John D.: On the Free Flight Motion of Missiles Having Slight Configurational Asymmetries. BRL Rep. 858, Aberdeen Proving Ground, 1953. (I. A. S. Preprint 395)

TABLE I.- CORRECTIONS TO MEASURED DRAG COEFFICIENTS; $M_\infty = 6.0$, $R_\infty = 6 \times 10^6$

Run no.	M_∞	$R_\infty \times 10^{-6}$	$\frac{1}{\alpha_T^2}$	C_D uncorrected	$\Delta C_{D_{le}}$	ΔC_{D_n}	ΔC_{D_b}	ΔC_{D_p} remaining pressure drag	ΔC_{D_F}	Total corrections	C_D corrected
(a) Smooth models											
49	5.23	5.74	0.00650	0.01581	0.00067	0	-0.00051	0.00002	-0.00013	0.00005	0.01586
157	6.49	7.56	.00409	.01157	.00047	.00003	.00038	-.00001	.00025	.00112	.01269
			.00407	.01129					.00025	.00112	.01241
168	6.11	6.88	.00359	.01338	.00007	.00001	-.00004	0	.00018	.00022	.01360
171	5.90	6.01	.00669	.01557	-.00002	.00003	-.00008	0	-.00001	-.00008	.01549
172	6.07	7.18	.00465	.01391	.00020	.00002	.00001	0	-.00021	-.00044	.01435
182	5.61	6.26	.02251	.02807	-.00012	.00003	-.00024	.00001	0	-.00032	.02775
			.02038	.02578					-.00001	-.00031	.02547
			.01958	.02591					0	-.00032	.02559
			.02642	.03070					0	-.00032	.03038
			.01770	.02370					.00001	-.00031	.02338
270	5.64	12.34	.00064	.01061	.00017	-.00003	-.00053	.00001	.00074	.00036	.01097
482	5.64	7.00	.00299	.01298	-.00017	-.00003	-.00038	.00001	.00017	-.00040	.01258
485	5.69	7.02	.00260	.01344	-.00031	-.00008	-.00029	.00001	.00017	-.00050	.01294
			.00348	.01377					.00017	-.00050	.01327
			.00212	.01338					.00016	-.00051	.01287
486	5.31	6.23	.00266	.01417	-.00021	0	-.00069	.00002	-.00001	-.00089	.01328
			.00287	.01398					.00001	-.00087	.01311
533	5.84	6.78	.00156	.01173	.00004	-.00003	-.00018	0	.00012	-.00005	.01168
543	5.24	12.25	.00612	.01613	-.00010	-.00022	-.00096	.00002	.00075	-.00051	.01562
544	5.49	6.41	.00628	.01672	.00025	-.00010	-.00051	.00001	.00002	-.00033	.01639
			.00762	.01732					.00002	-.00033	.01699
			.00562	.01622					.00002	-.00033	.01589
			.00621	.01674					.00001	-.00034	.01640
			.00455	.01566					0	-.00035	.01531
(b) Rough models											
181	5.68	5.92	.01298	.02240	-.00032	.00002	-.00022	.00001	-.00009	-.00060	.02180
			.01606	.02407					-.00008	-.00059	.02348
			.00905	.02020					-.00010	-.00061	.01959
			.01710	.02535					-.00009	-.00060	.02475
			.01350	.02240					-.00009	-.00060	.02180
			.00903	.02010					-.00010	-.00061	.01949
183	5.90	6.58	.00399	.01402	-.00005	.00003	-.00008	0	.00010	0	.01402
			.00352	.01435					.00011	.00001	.01436
269	5.29	5.89	.01960	.03206	-.00006	-.00001	-.00064	.00002	-.00033	-.00102	.03104
			.01650	.02860					-.00028	-.00097	.02763
			.01400	.02493					-.00021	-.00090	.02403
			.01685	.02960					-.00030	-.00099	.02861
			.01997	.03220					-.00033	-.00102	.03118
			.01731	.02958					-.00029	-.00098	.02860
271	5.33	5.99	.00218	.01571	.00021	-.00005	-.00050	.00001	-.00015	-.00048	.01523
276	5.43	11.65	.00130	.01360	.00036	-.00032	-.00074	.00001	.00073	.00004	.01364
372	5.87	6.33	.00215	.01384	.00052	-.00003	.00008	0	.00006	.00063	.01447
487	5.49	6.73	.00013	.01171	-.00007	-.00014	-.00049	.00001	.00010	-.00059	.01112
488	5.49	6.54	.00281	.01362	-.00005	-.00006	-.00036	.00001	.00005	-.00041	.01321
			.00410	.01467					.00006	-.00040	.01427
			.00228	.01333					.00006	-.00040	.01293
493	5.92	6.42	.00223	.01336	.00003	-.00003	.00003	0	.00007	.00010	.01346
495	5.91	13.91	.00179	.01180	.00026	-.00007	-.00031	0	.00090	.00078	.01258
537	5.86	6.80	.00421	.01502	.00009	-.00005	-.00019	0	.00014	-.00001	.01501
			.00363	.01410					.00014	-.00001	.01409
			.00344	.01366					.00014	-.00001	.01365
			.00371	.01495					.00014	-.00001	.01494
			.00392	.01415					.00014	-.00001	.01414
			.00408	.01473					.00014	-.00001	.01472
540	5.53	15.66	.00032	.01259	-.00001	0	-.00091	.00001	.00103	.00012	.01271
541	5.75	6.93	.00440	.01368	.00015	-.00005	-.00031	0	.00017	-.00004	.01364
597	5.70	6.51	.00082	.01257	0	-.00013	-.00036	.00001	.00006	-.00042	.01215
598	5.82	6.91	.00289	.01422	.00004	-.00010	-.00029	0	.00015	-.00020	.01402
599	5.75	6.44	.00231	.01405	.00001	-.00009	-.00031	0	.00006	-.00033	.01372

TABLE II.- ROOT-MEAN-SQUARE DEVIATION OF EXPERIMENTAL DATA FROM
THEORETICAL MOTION CURVES

Run no.	Deviation in α and β , deg	Deviation in y and z, in.
168	0.23	0.0082
181	.14	.0105
257	.20	.0076
269	.26	.0073
482	.05	.0048
486	.15	.0023
488	.09	.0041
493	.05	.0035
540	.13	.0064
541	.09	.0102
599	.10	.0031

A
2
4
0

Body fineness ratio 9.5
Nose, tangent ogive of fineness ratio 5, with tip blunted to spherical diameter of .010
All dimensions in inches

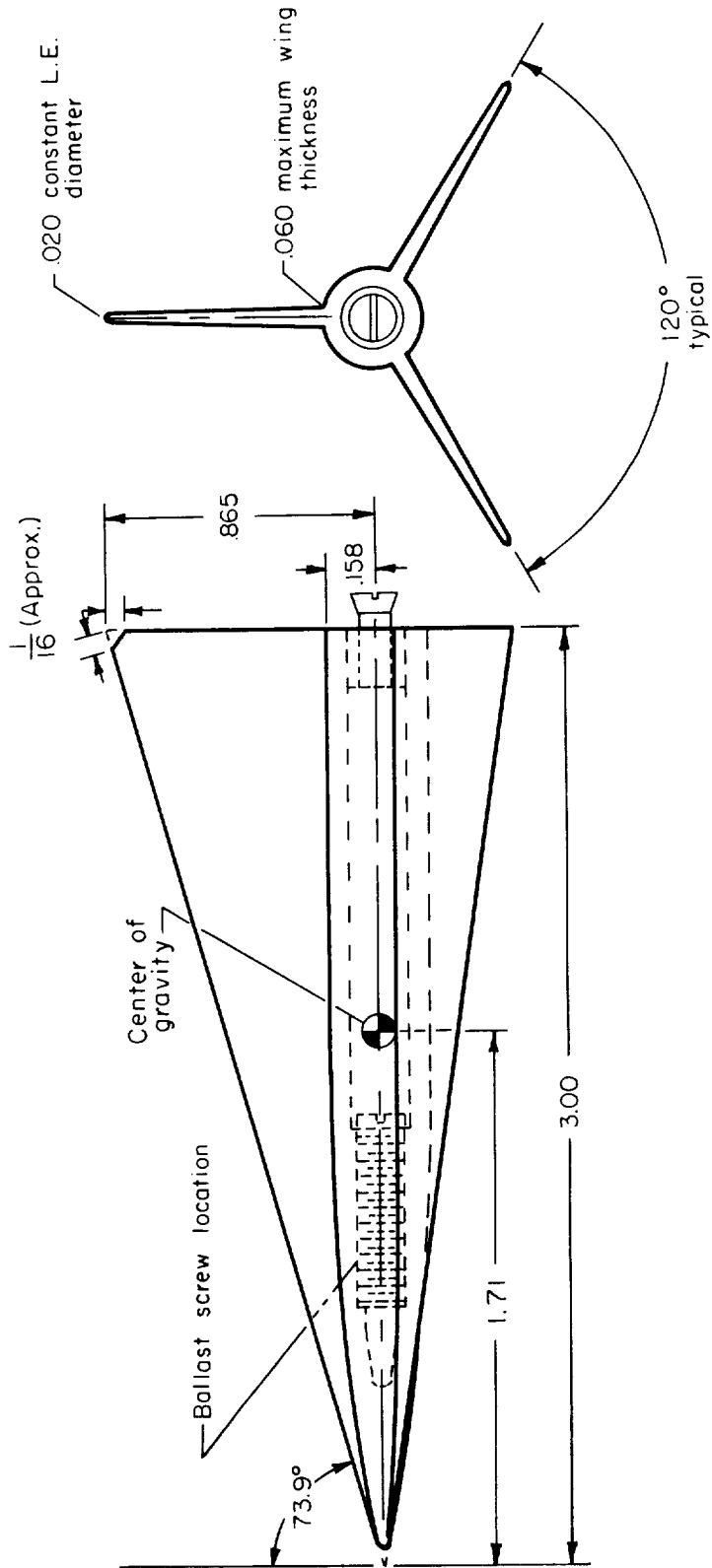
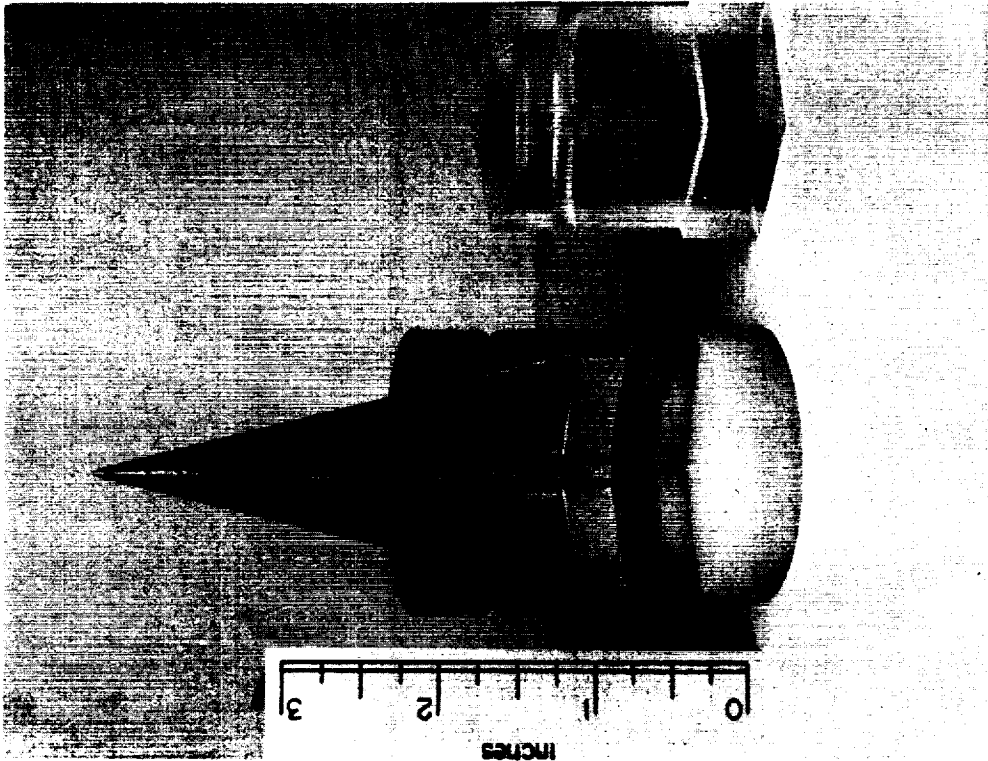
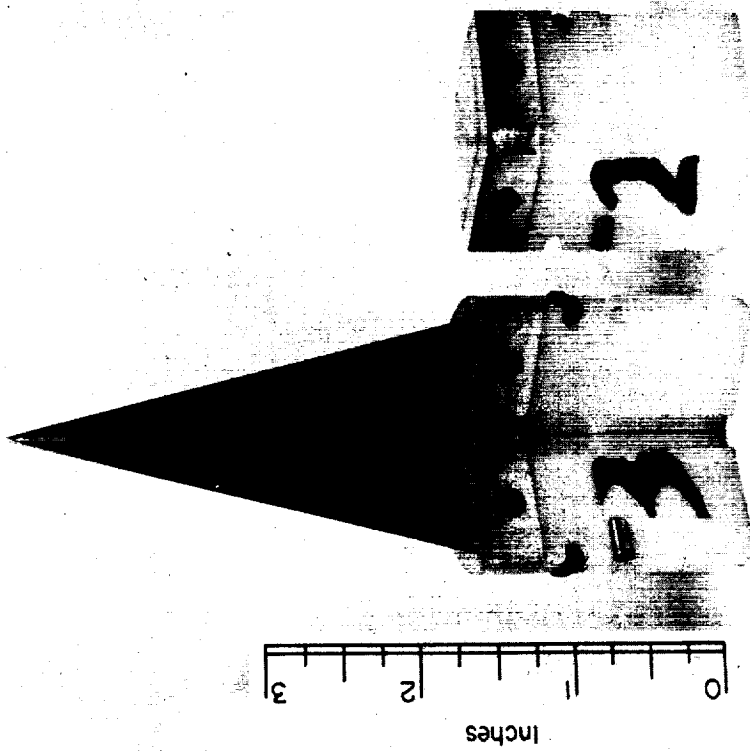


Figure 1.- Nominal model dimensions.



A-26667

(a) Model and partially assembled sabot.

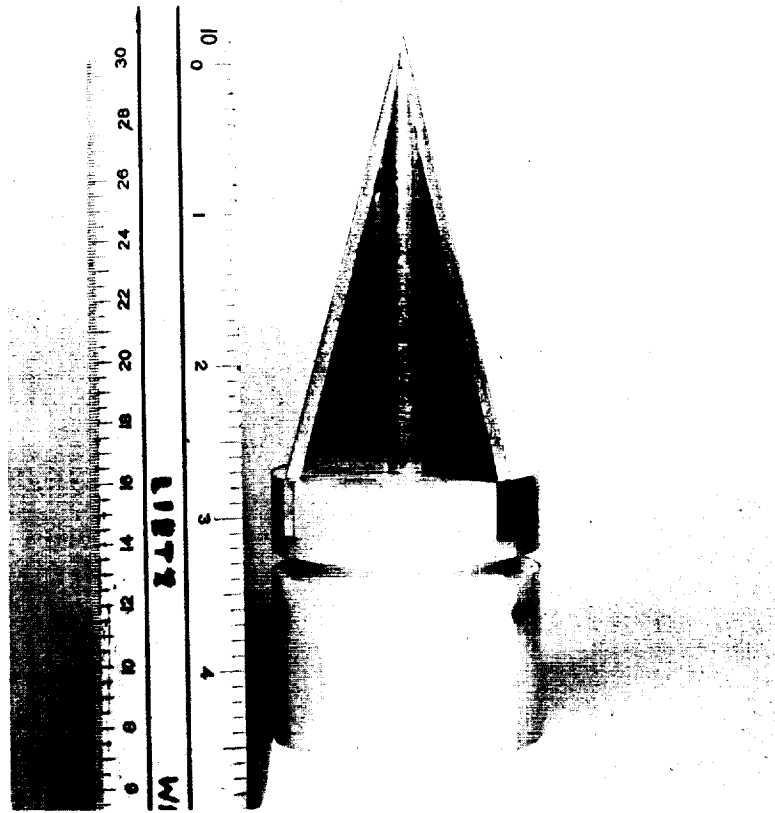


A-26669

(b) Model and partially assembled sabot.

Figure 2.- Photographs of models, sabots, and roughness elements.

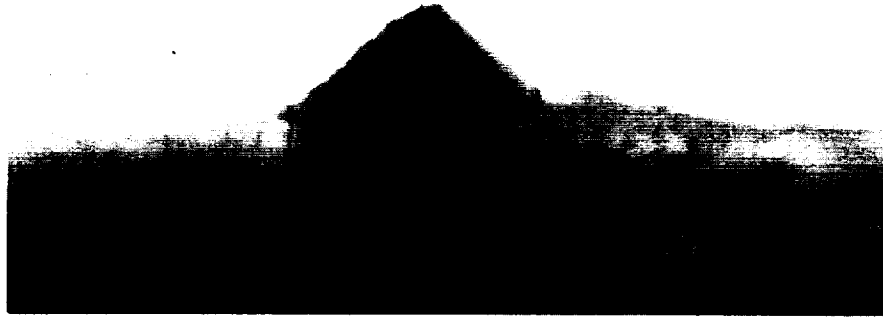
A
2
4
0



A-26668

(c) Model and sabot assembly.

Figure 2.- Continued.



(d) Side view of roughness element produced with punch; 100X.



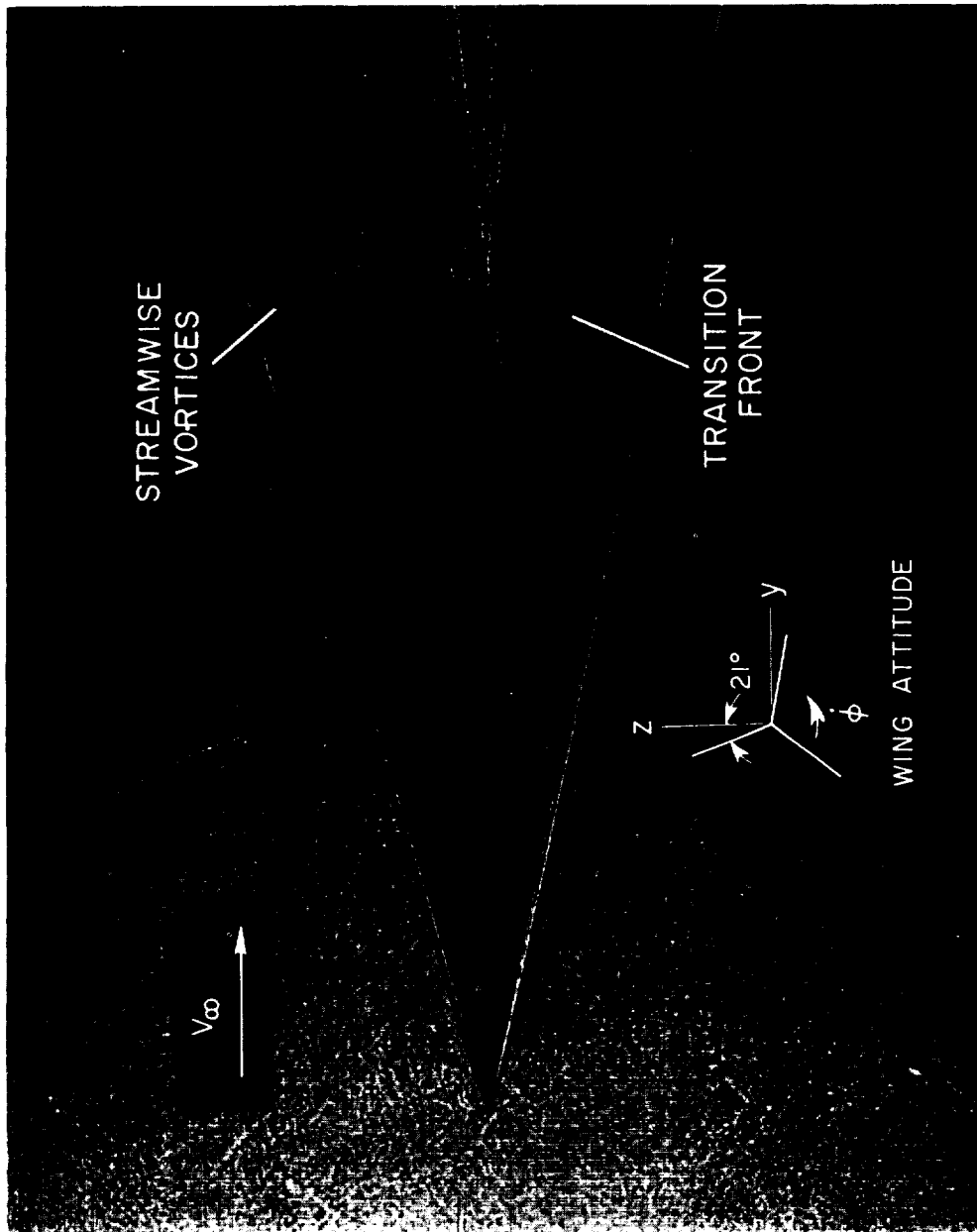
(e) Plan form of punch mark. Raised portion is dark area at right end; 100X.



(f) Profile of notch filed in wing leading edge; 100X.

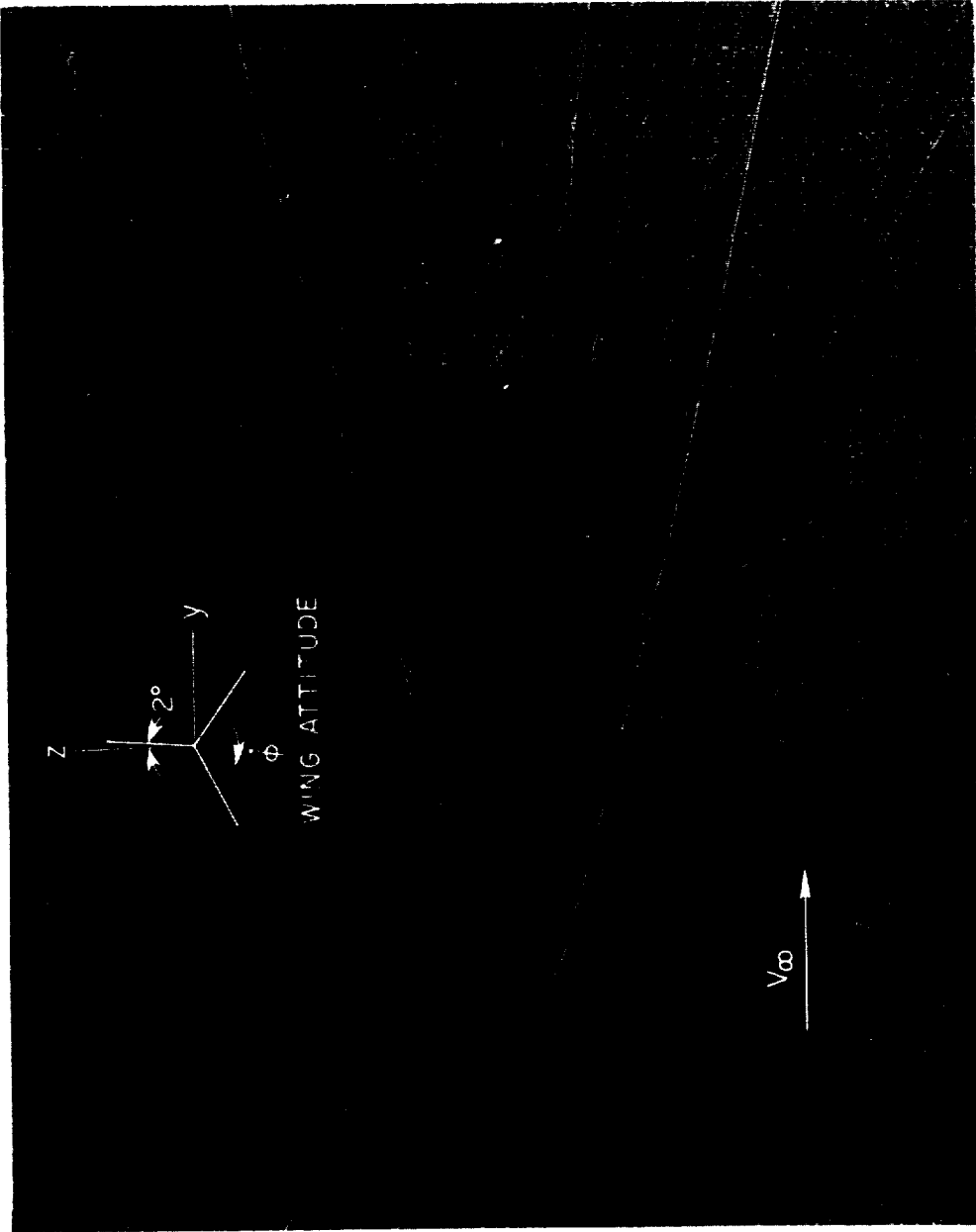
Figure 2.- Concluded.

A
2
4
0



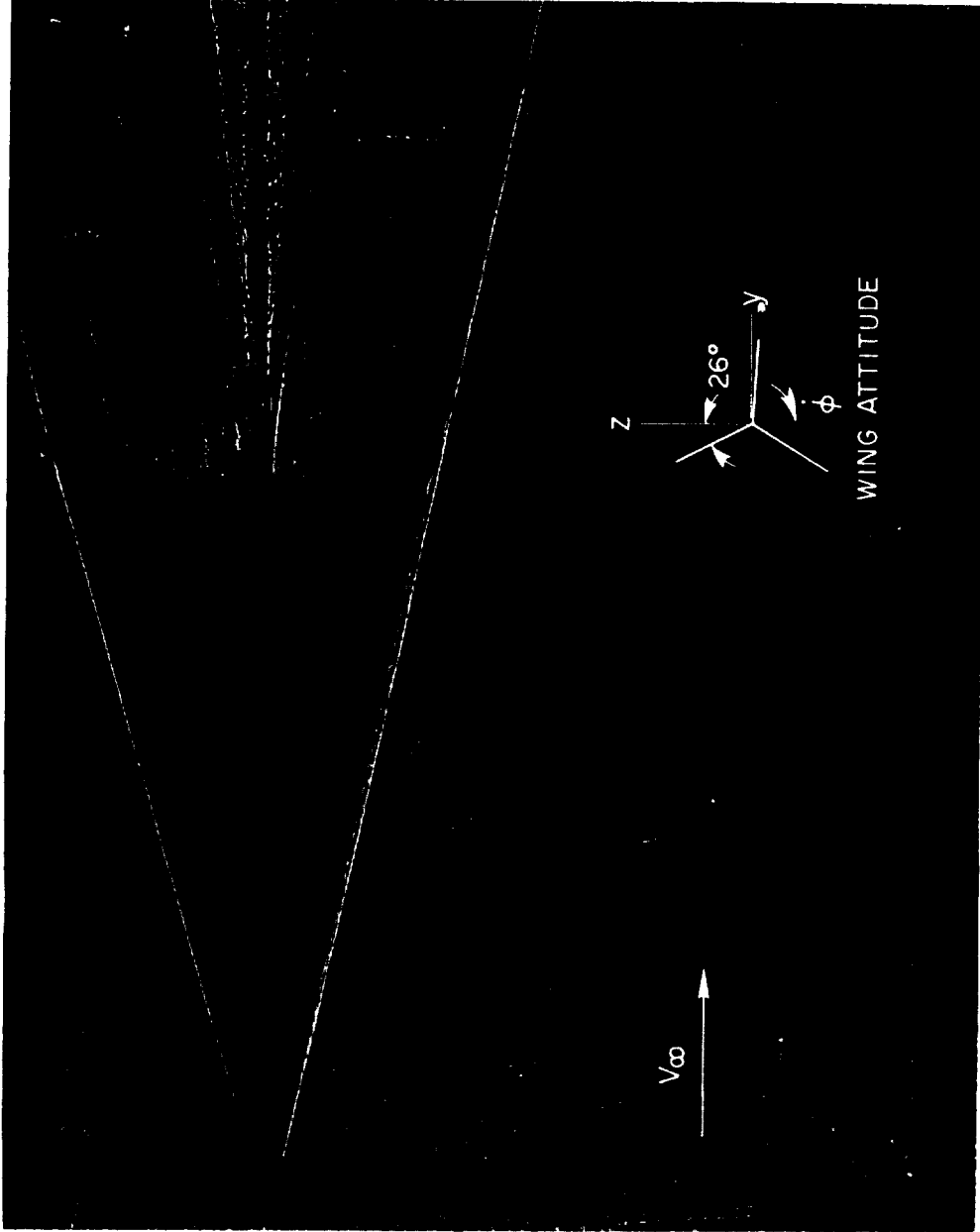
(a) Run 168; smooth model; $\alpha = -4.2^\circ$; $\alpha_T = 4.7^\circ$; $M_\infty = 6.11$; $R_\infty = 6.88 \times 10^6$.

Figure 3.- Shadowgraphs of models in flight.



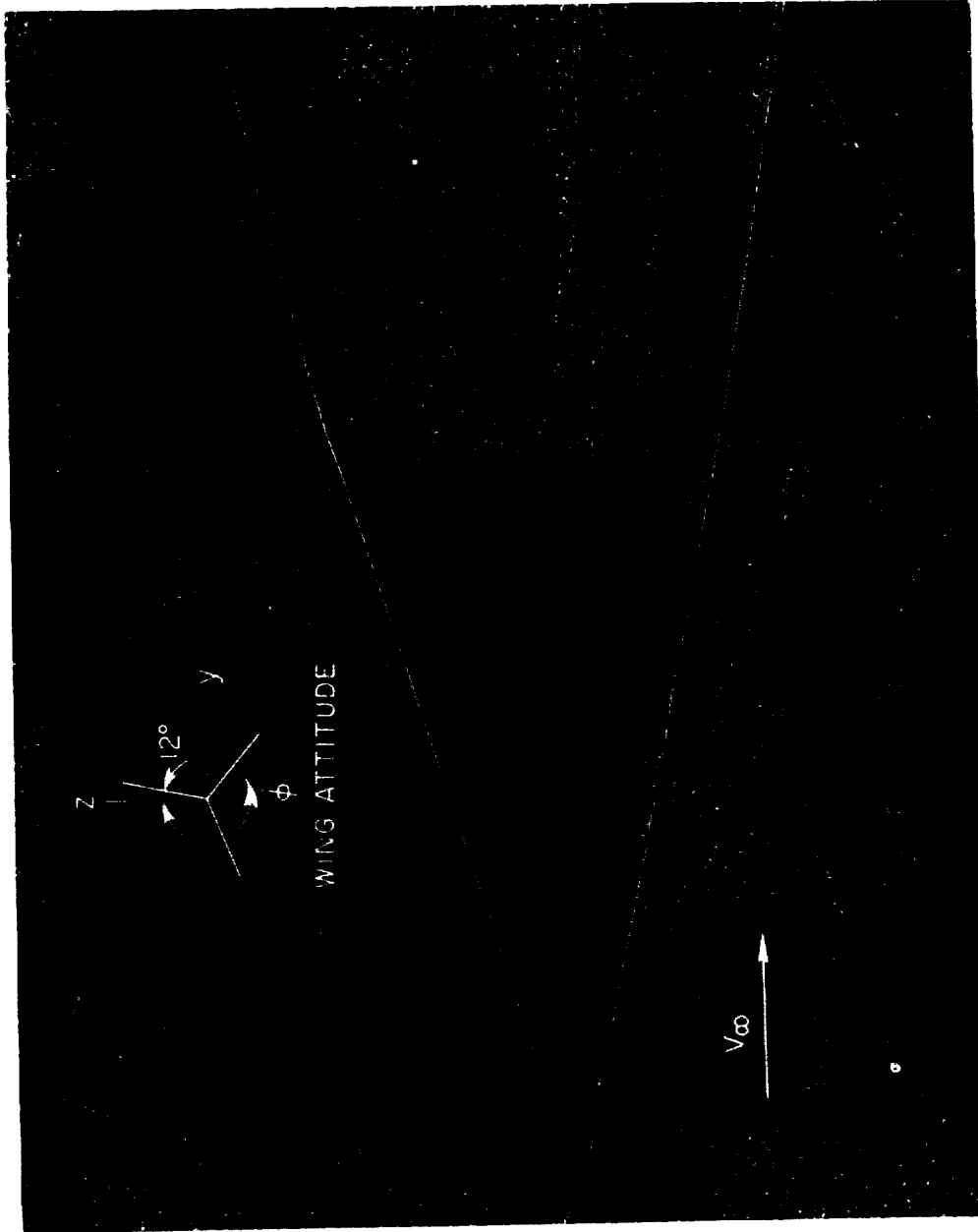
(b) Run 488; rough model; $\alpha = 2.4^\circ$; $\alpha_T = 3.2^\circ$; $M_\infty = 5.49$; $R_\infty = 6.54 \times 10^6$.

Figure 3.- Continued.



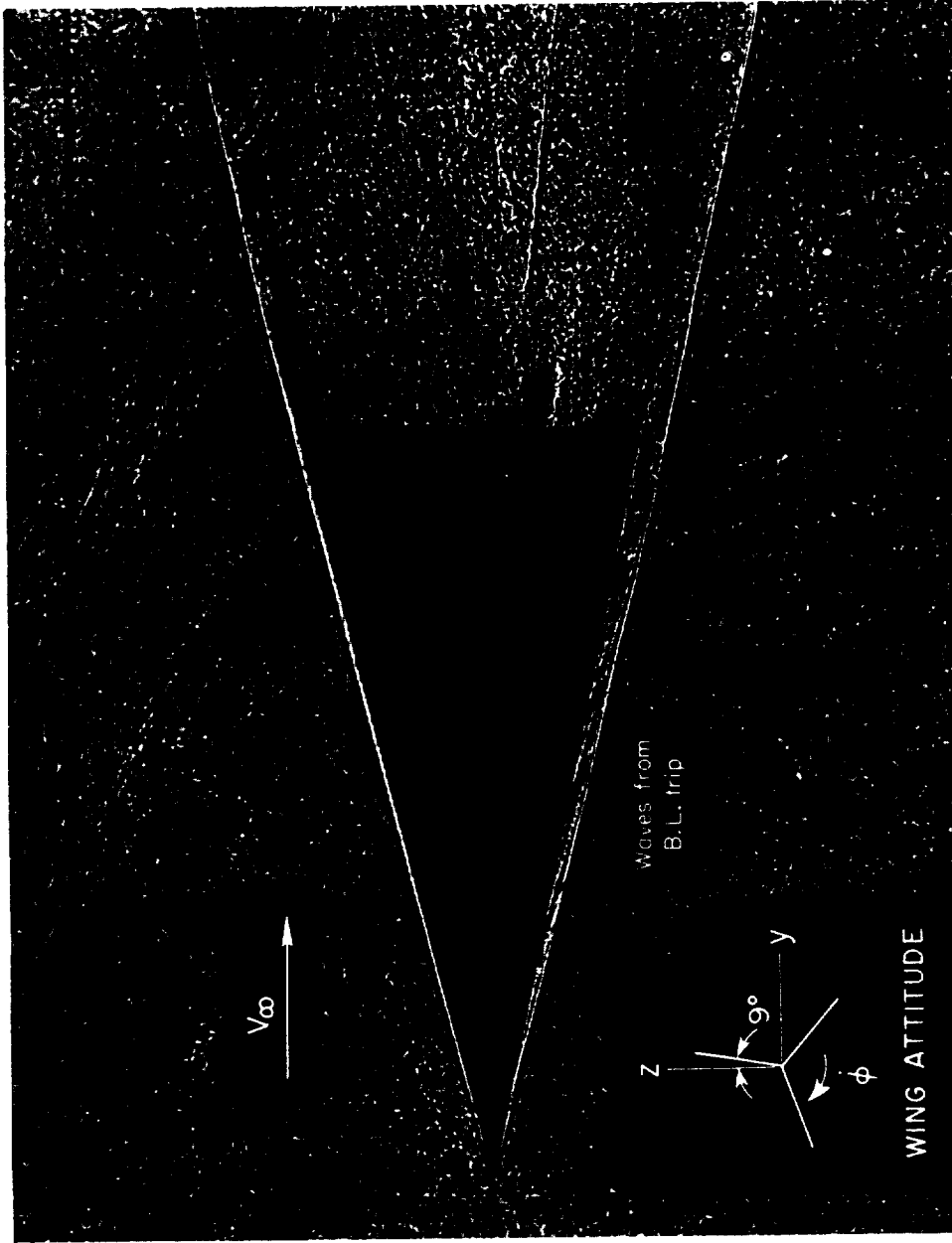
(c) Run 493; rough model with sandblasted leading edge; $\alpha = -1.8^\circ$;
 $\alpha_r = 3.6^\circ$; $M_\infty = 5.92$; $R_\infty = 6.42 \times 10^6$.

Figure 3.- Continued.



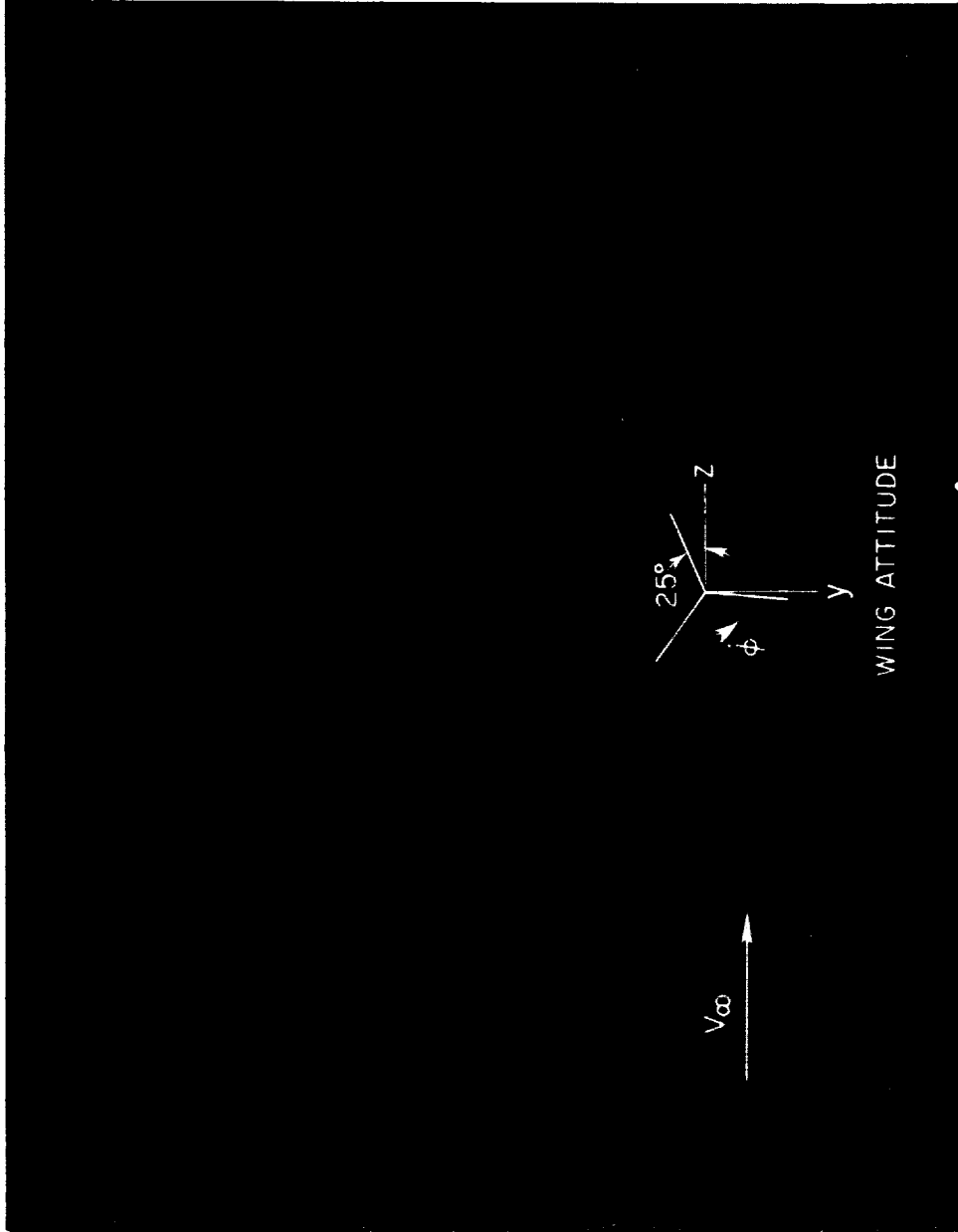
(d) Run 537; rough model with burrs 0.002 inch high along leading edge;
 $\alpha = -0.6^\circ$; $\alpha_T = 0.8^\circ$; $M_\infty = 0.80$; $M_0 = 5.86$; $R_0 = 6.80 \times 10^6$.

Figure 3.- Continued.



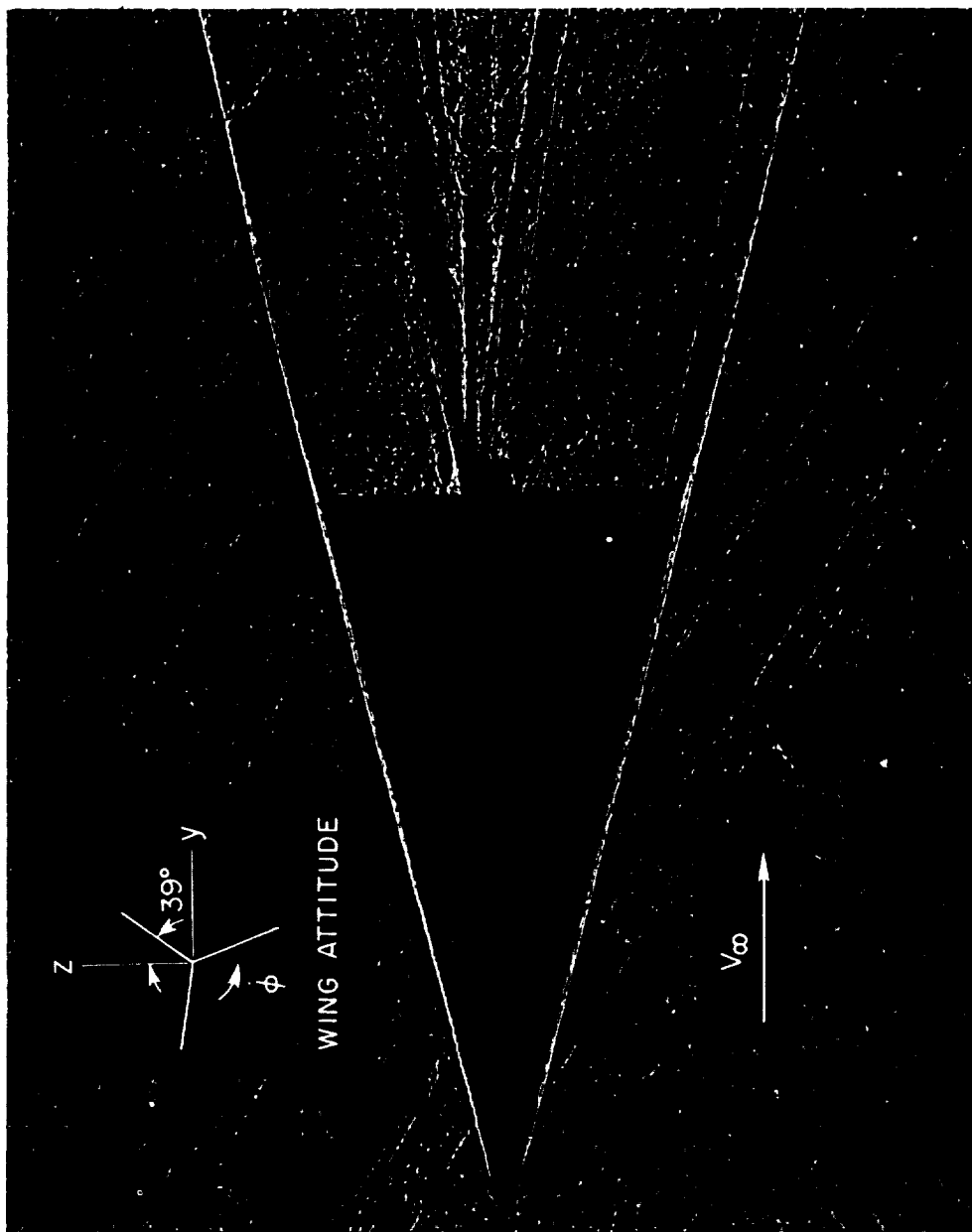
(e) Run 599; rough model with burrs 0.006 inch high along leading edge;
 $\alpha = 1.0^\circ$; $\alpha_r = 1.2^\circ$; $M_\infty = 5.75$; $R_\infty = 6.44 \times 10^6$.

Figure 3.- Continued.



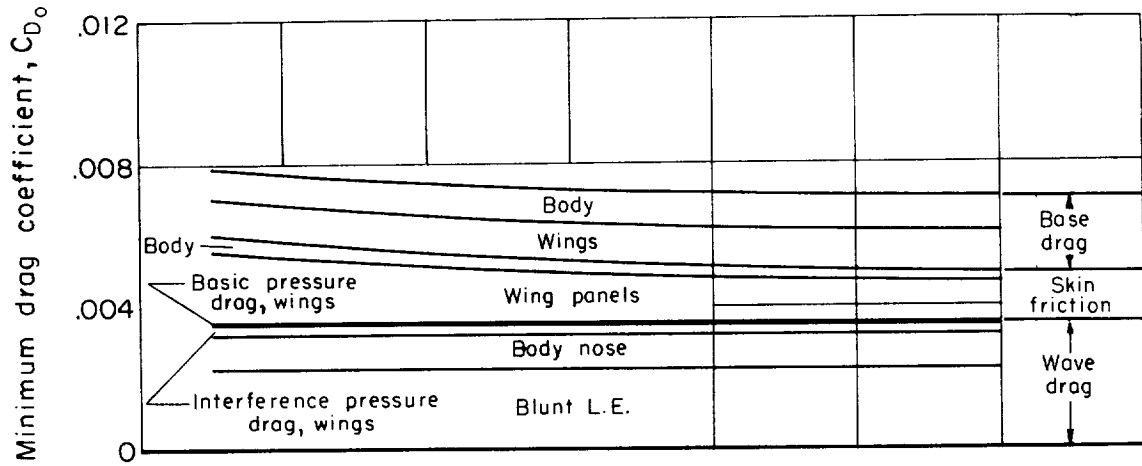
(f) Run 269; rough model with notches along leading edge; $\beta = 7.1^\circ$;
 $\alpha_T = 9.0^\circ$; $M_\infty = 5.29$; $R_\infty = 5.89 \times 10^6$.

Figure 3.- Continued.

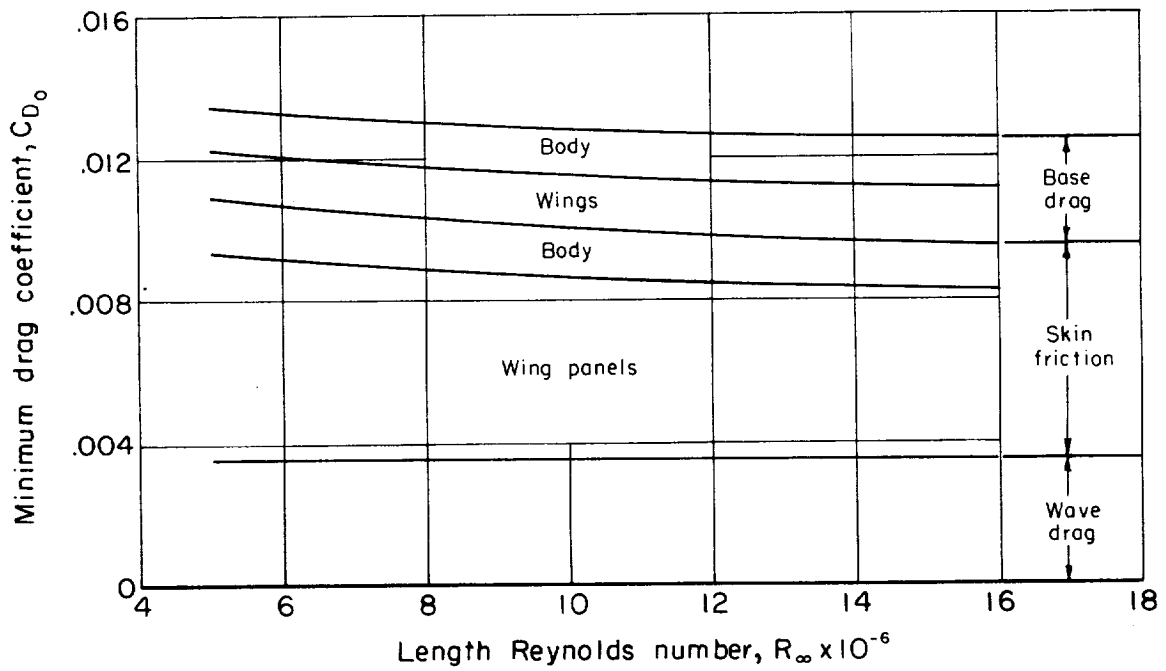


(g) Run 276; rough model; $\alpha = -1.3^\circ$; $\alpha_T = 1.3^\circ$; $M_\infty = 5.43$; $R_\infty = 11.65 \times 10^6$.

Figure 3.- Concluded.



(a) Laminar



(b) Turbulent

Figure 4.- Estimates of minimum drag coefficient at $M_\infty = 6$ as a function of length Reynolds number.

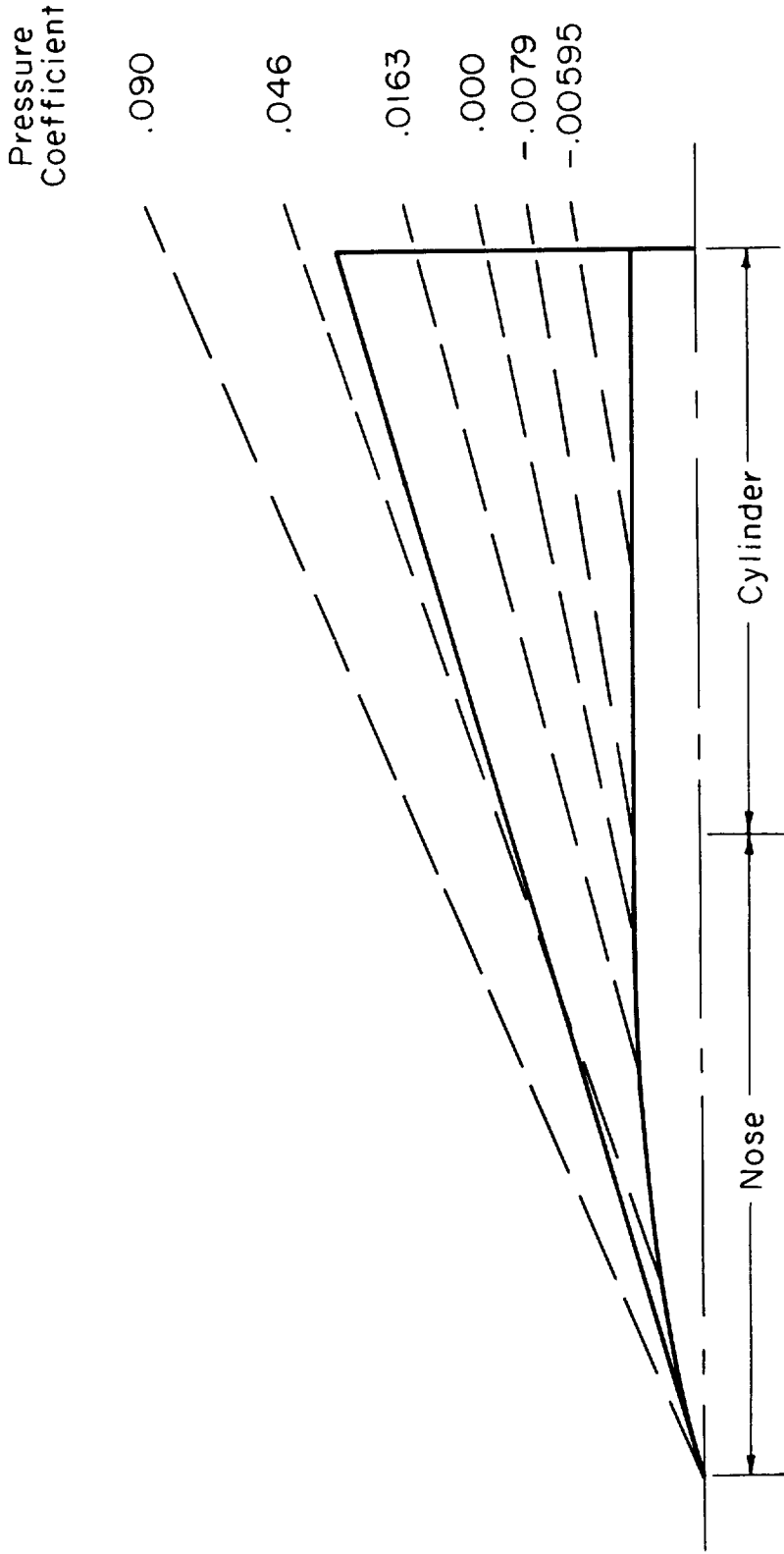


Figure 5.- Interference pressure distribution assumed for wing panel; $M_\infty = 6$.

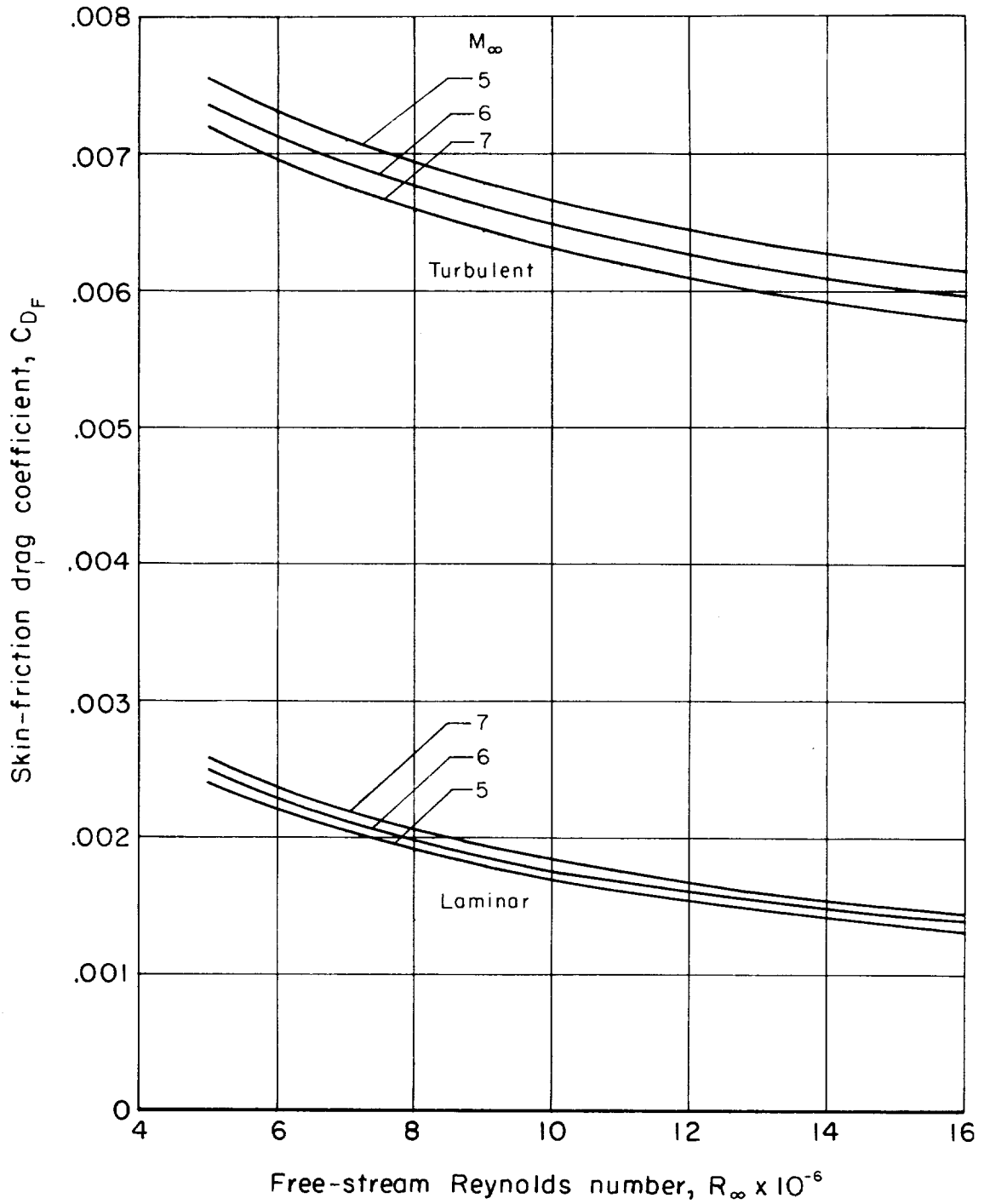


Figure 6.- Estimated skin friction drag coefficients.

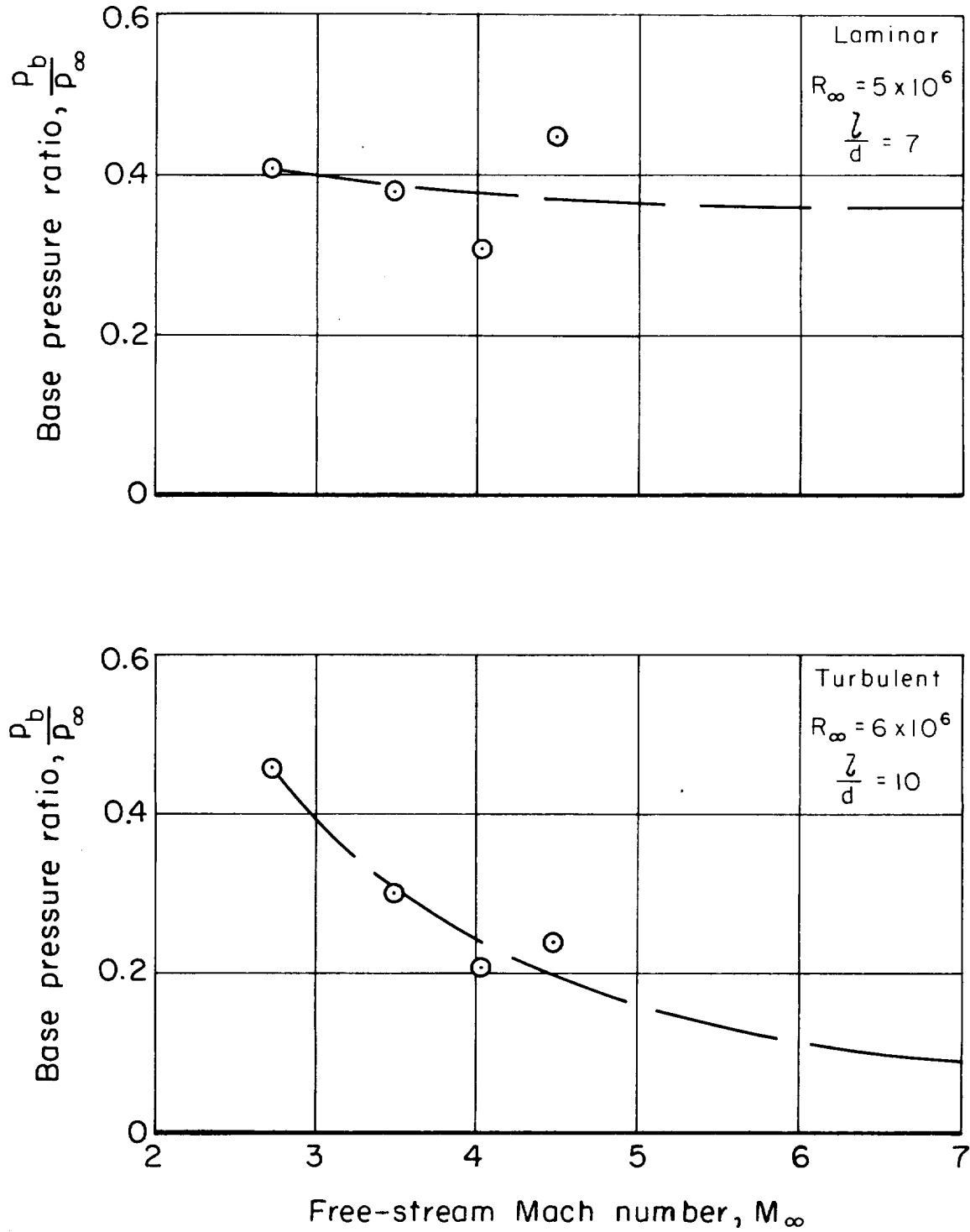


Figure 7.- Base pressure data from reference 14 and fairings used in present estimates.

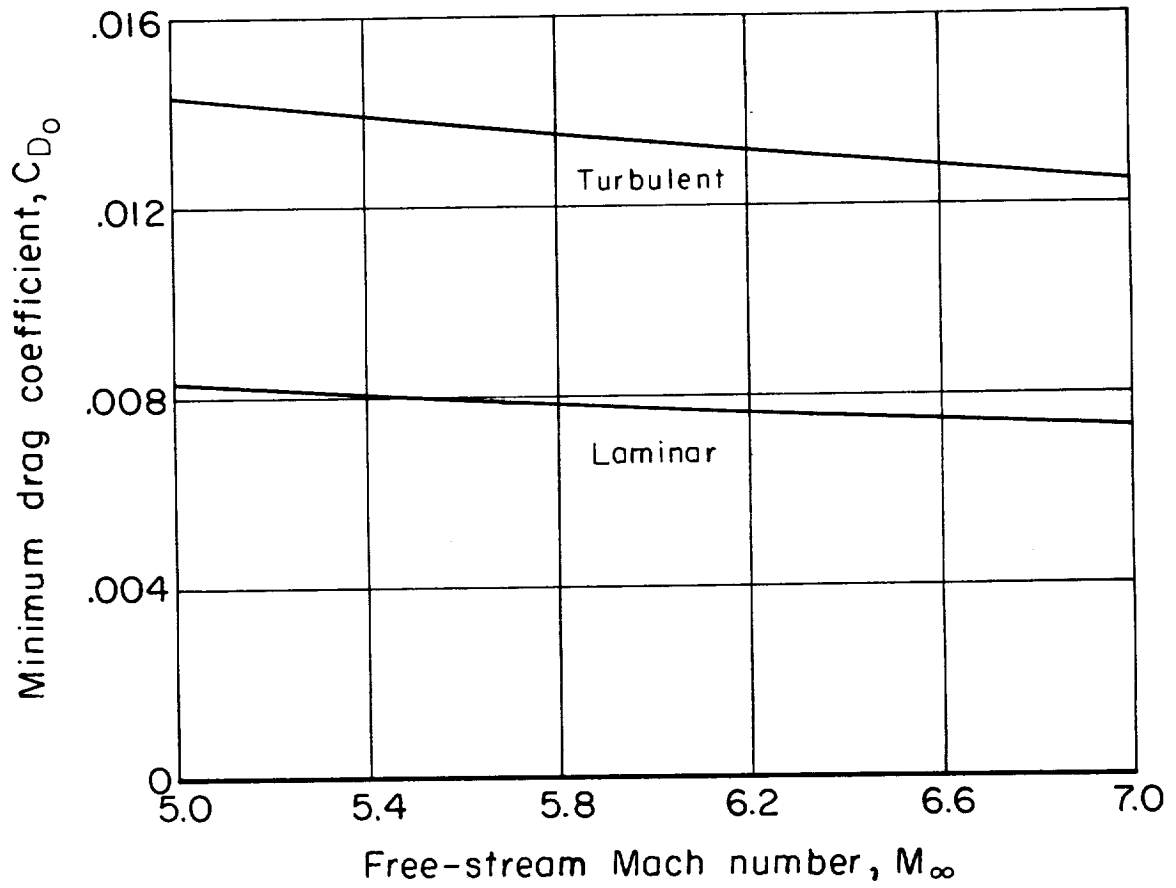
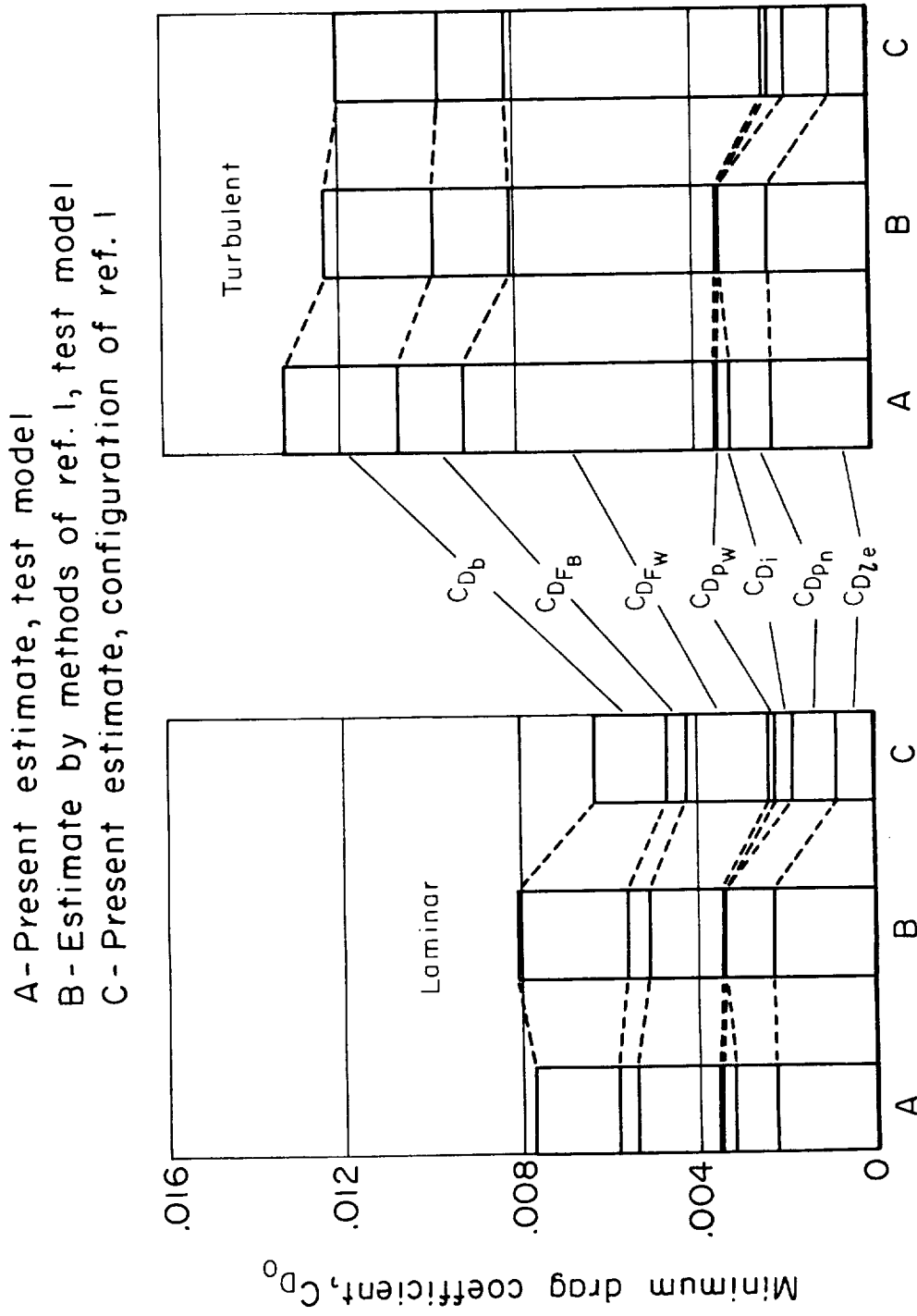
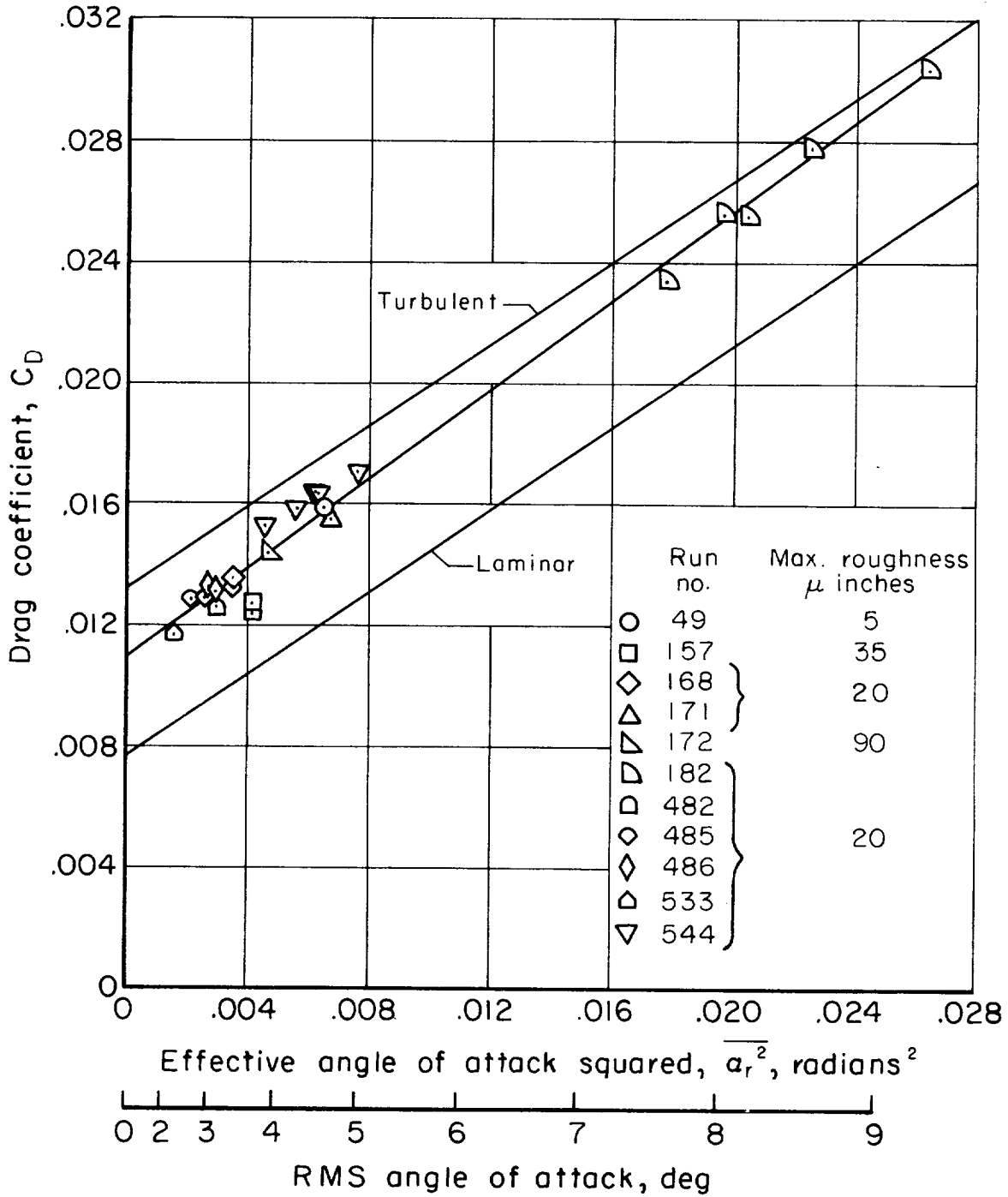


Figure 8.- Estimated minimum drag coefficient as a function of Mach number at $R_\infty = 6 \times 10^6$.



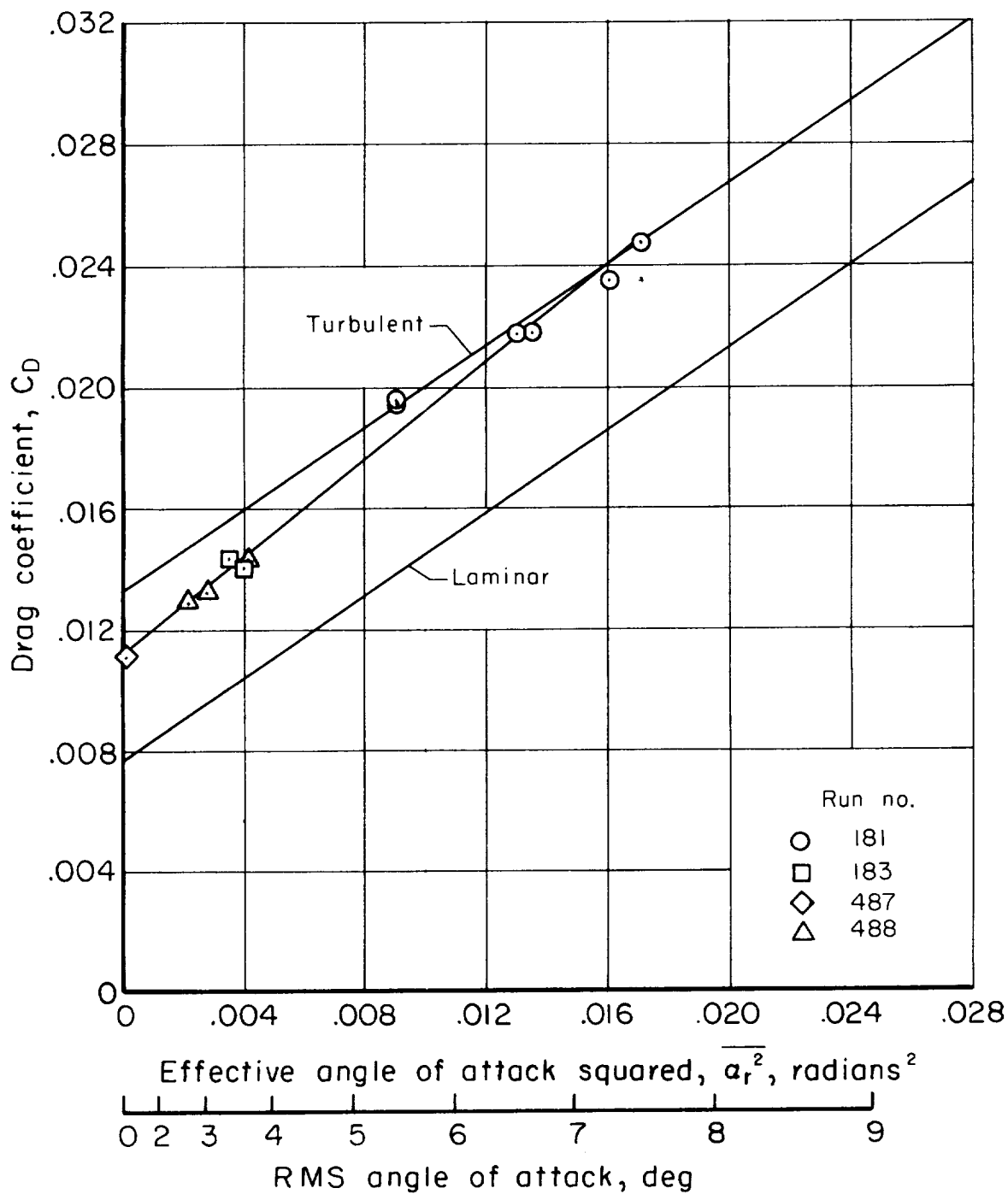
- A - Present estimate, test model
- B - Estimate by methods of ref. 1, test model
- C - Present estimate, configuration of ref. 1

Figure 9.- Comparison of present drag estimate with estimate and configuration of reference 1.



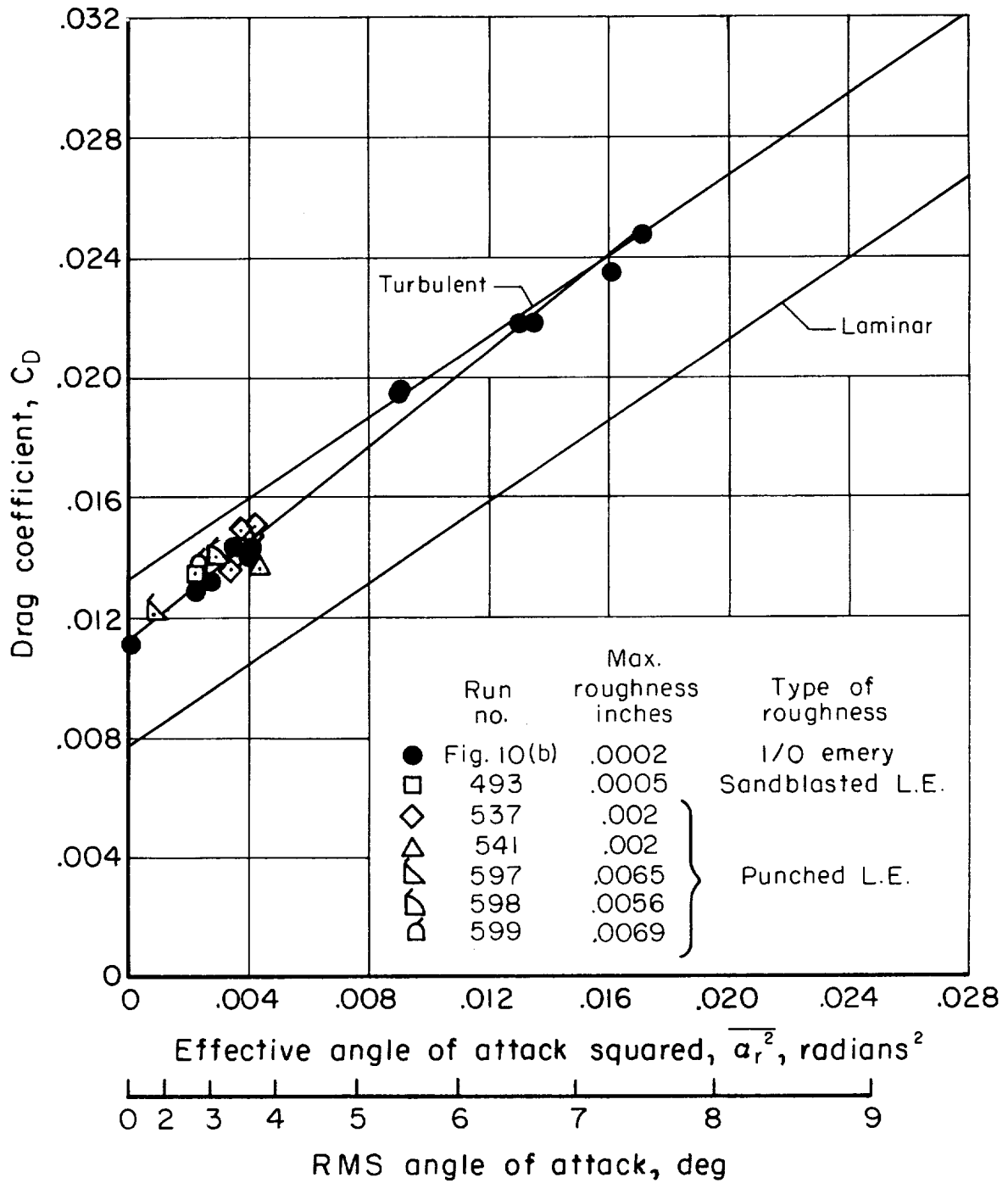
(a) Smooth models.

Figure 10.- Variation of drag coefficient with the effective angle of attack squared; $M_\infty = 6$, $R_\infty = 6 \times 10^6$.



(b) Rough models finished with 1/0 emery cloth (max. roughness 200 μ m.).

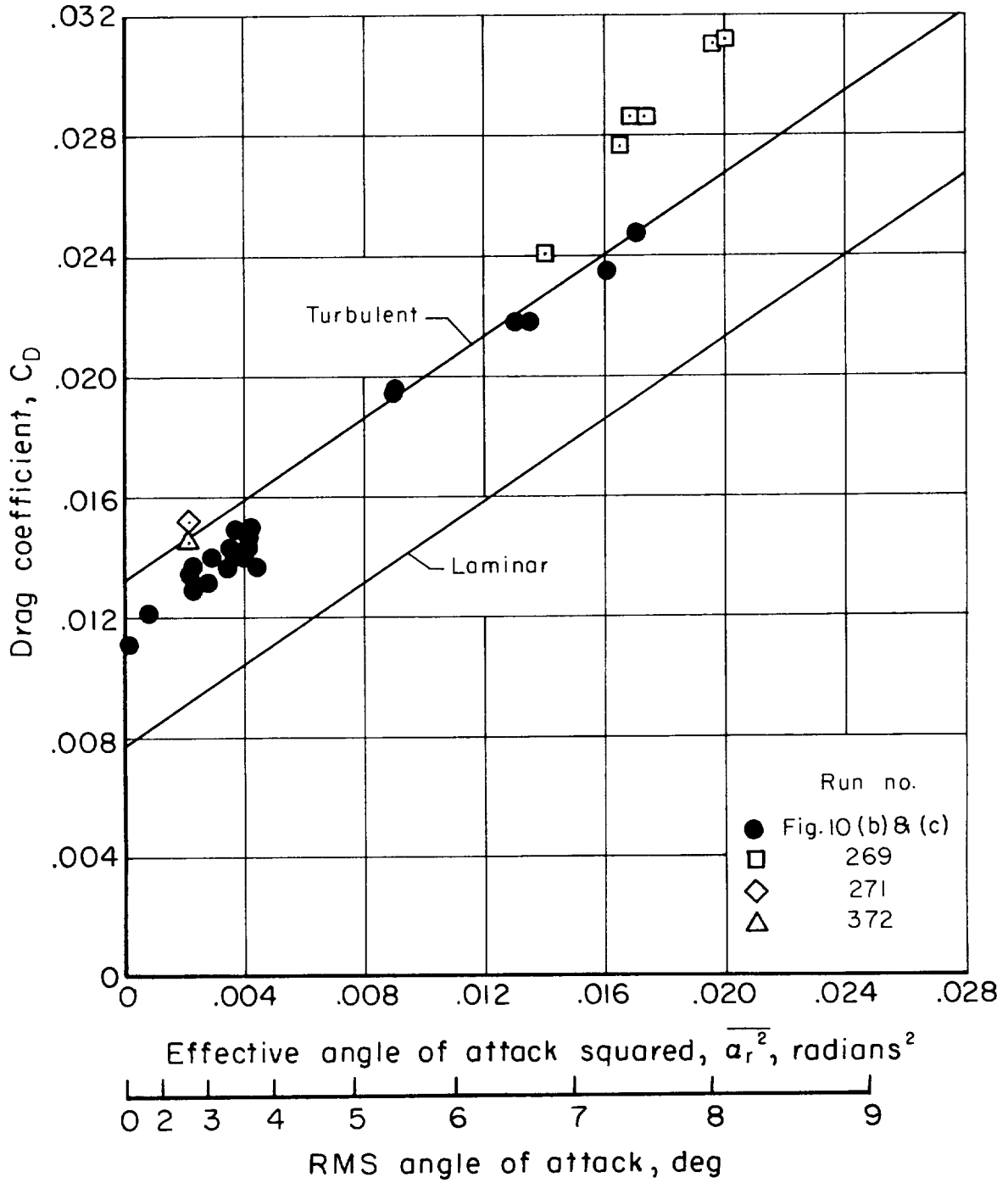
Figure 10.- Continued.



(c) Rough models with additional roughness as noted.

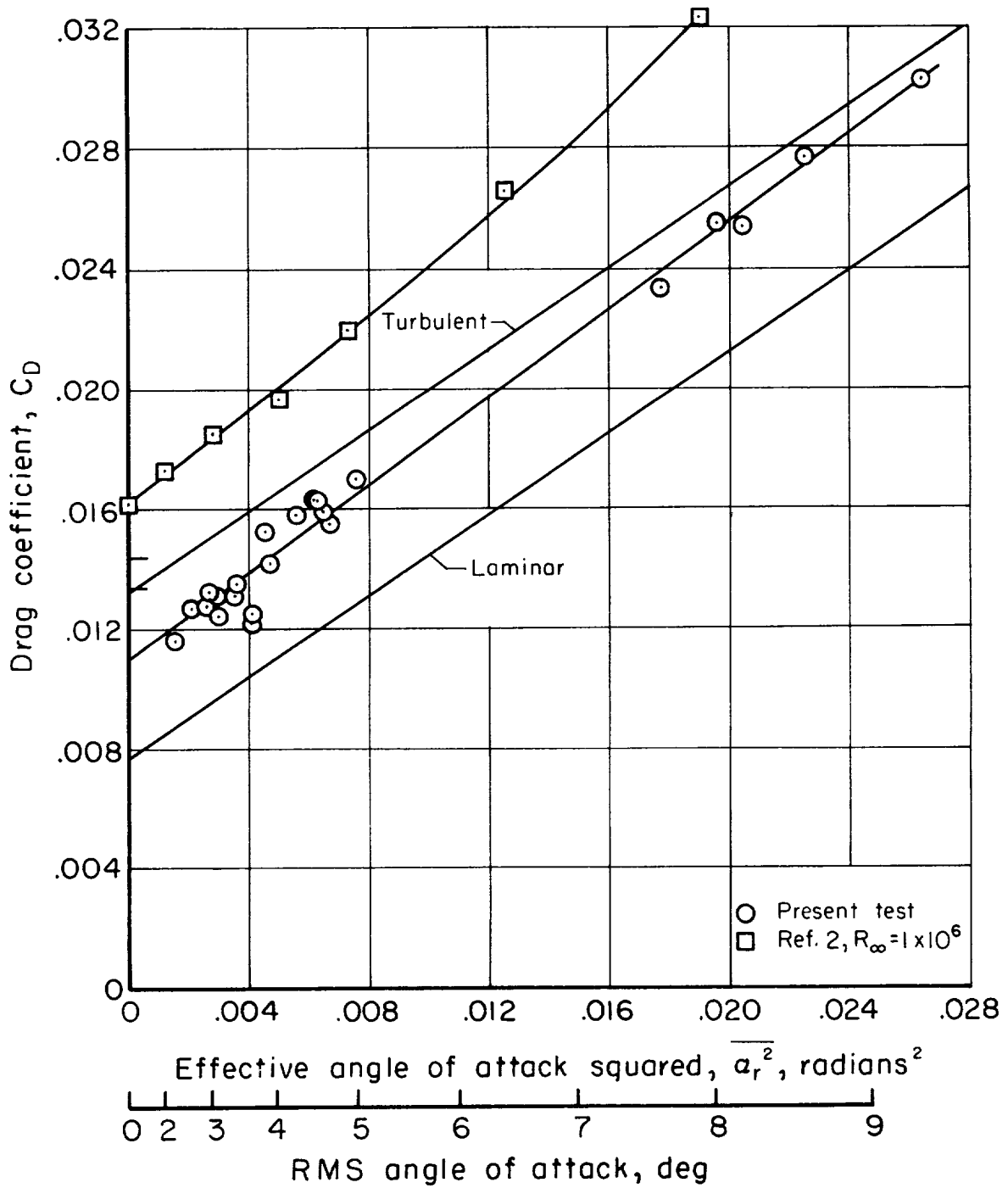
Figure 10.- Continued.

A
2
4
0



(d) Rough models with notched leading edges (notches approximately 0.006 inch deep).

Figure 10.- Continued.

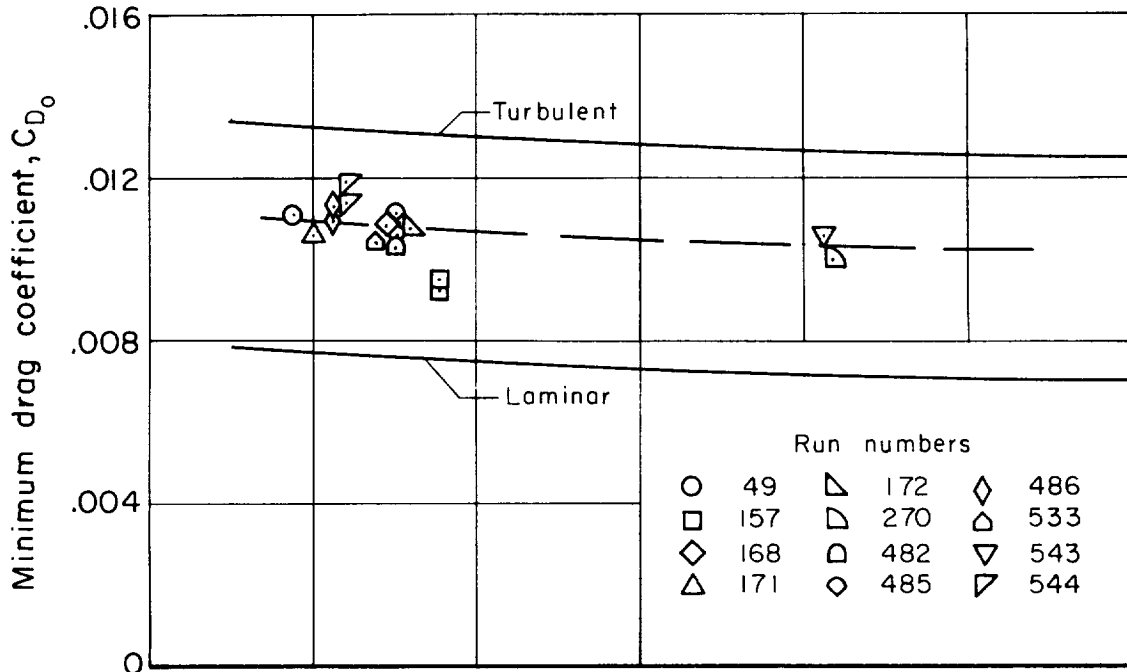


A
2
4
0

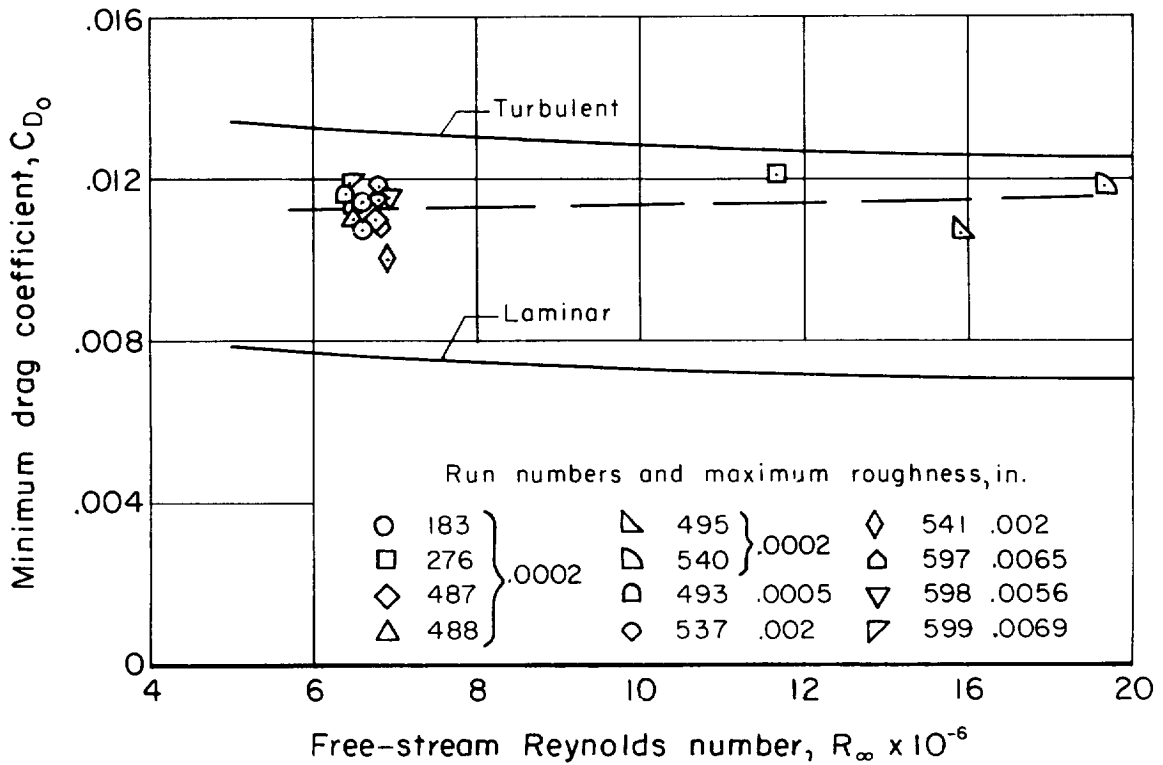
(e) Comparison of smooth-model data with that of reference 2.

Figure 10.- Concluded.

A
2
4
0



(a) Smooth models.



(b) Rough models with additional roughness as noted.

Figure 11.- Variation of minimum drag coefficient with Reynolds number, $M_\infty = 6$.

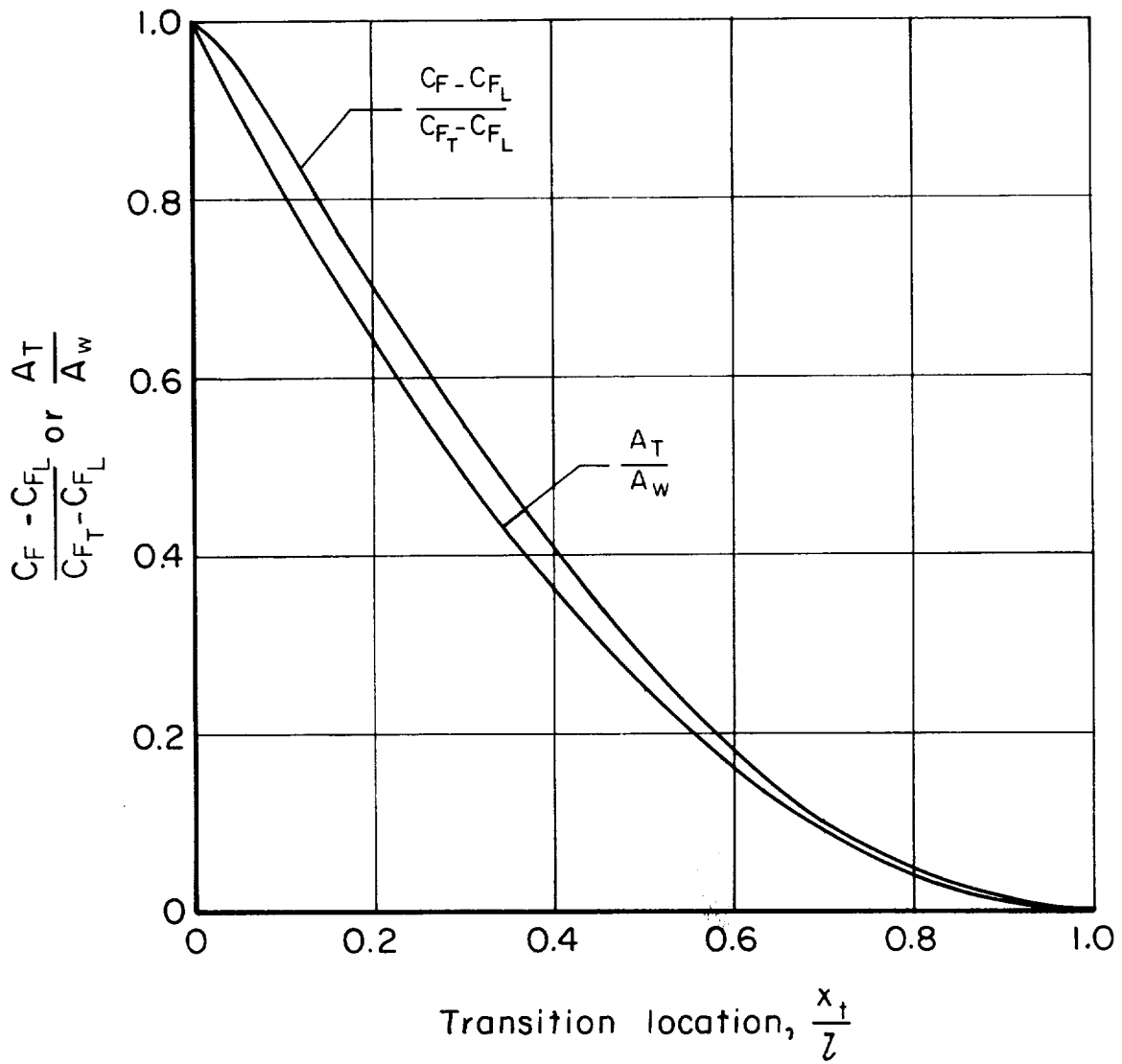
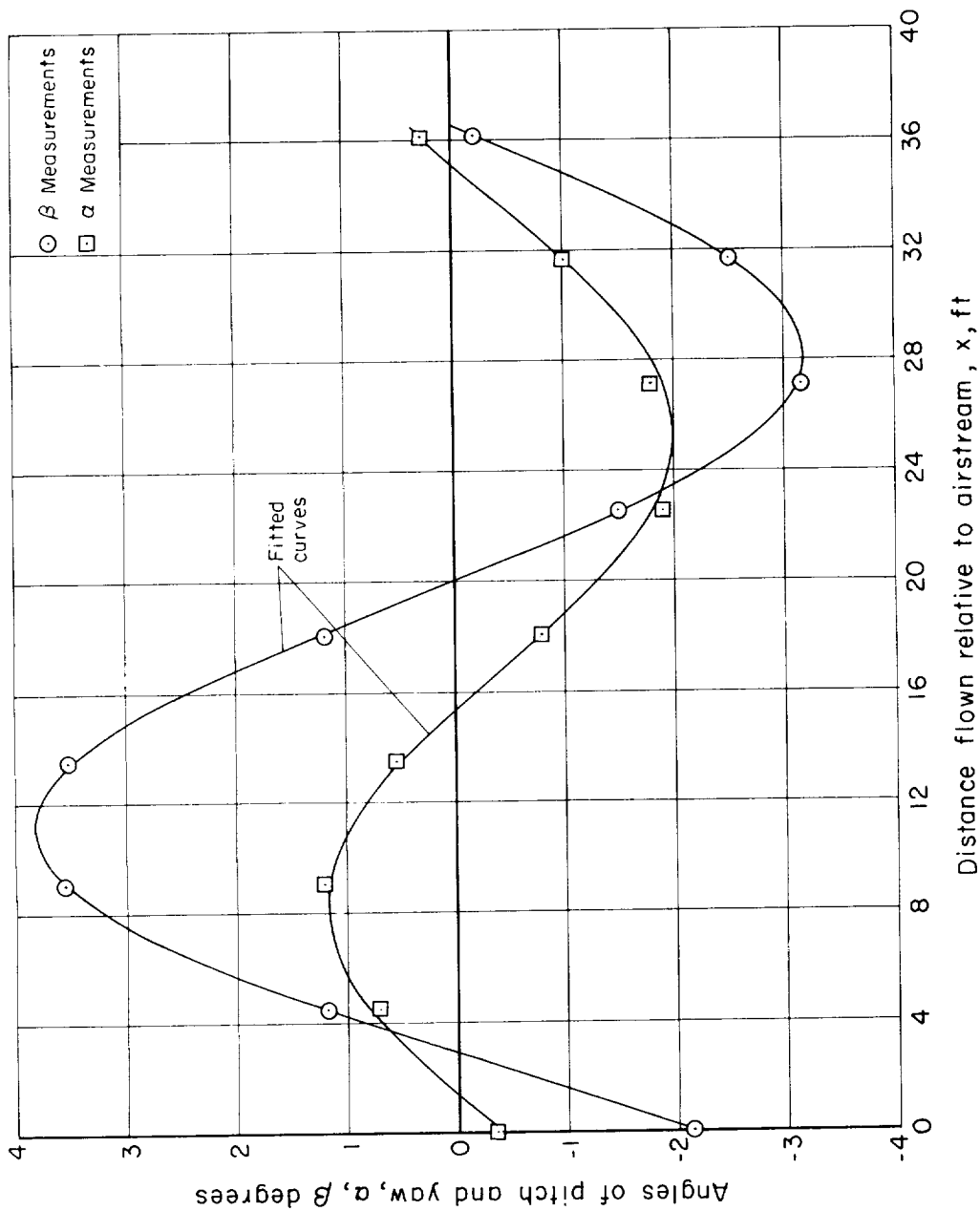
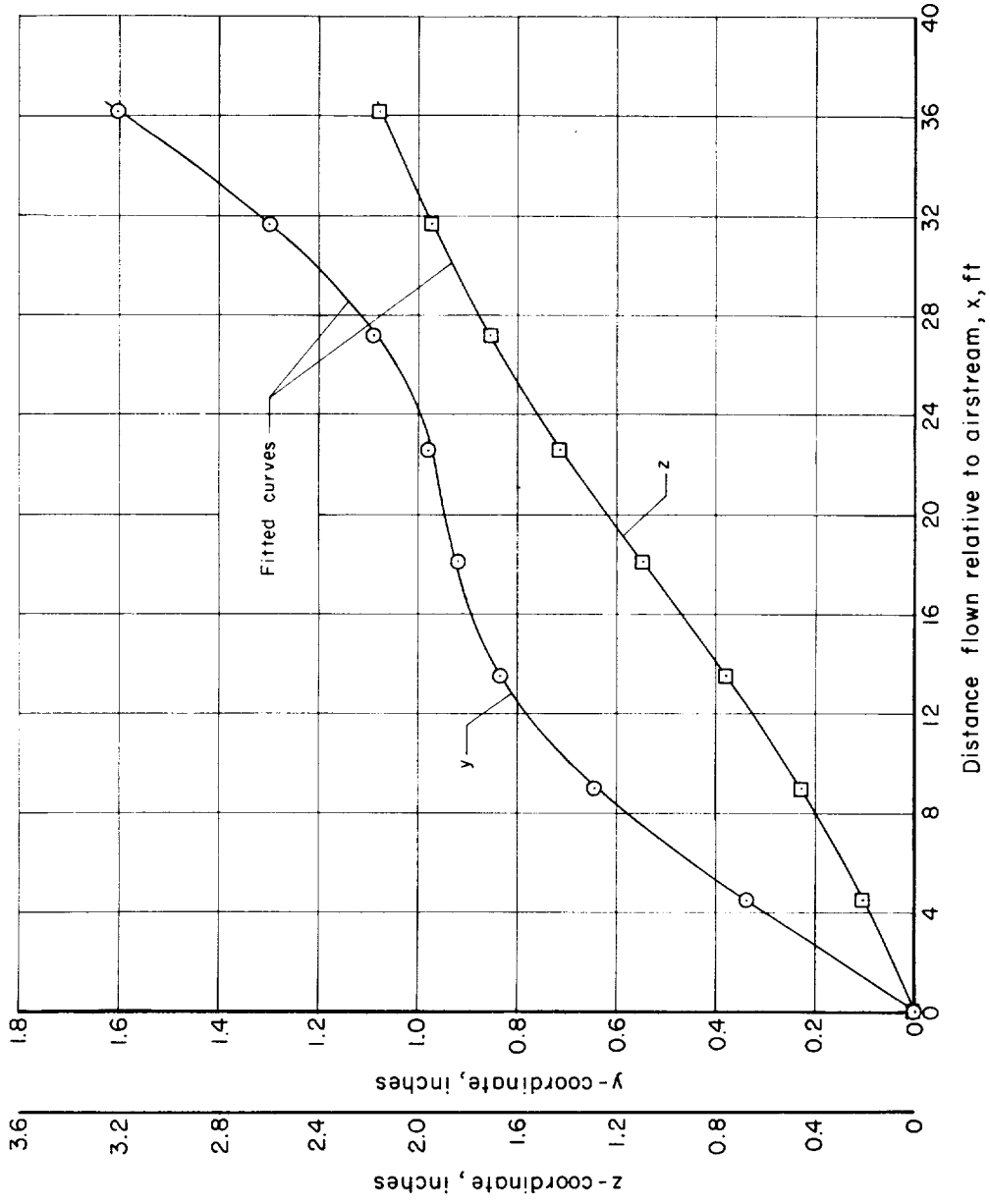


Figure 12.- Effect of transition location on skin-friction coefficient.



(a) Angles of pitch and yaw as a function of x.

Figure 13.- Fit of theoretical motion equations to experimental data; run 493.



(b) Swerving motion in y and z planes as a function of x.

Figure 13.- Concluded.

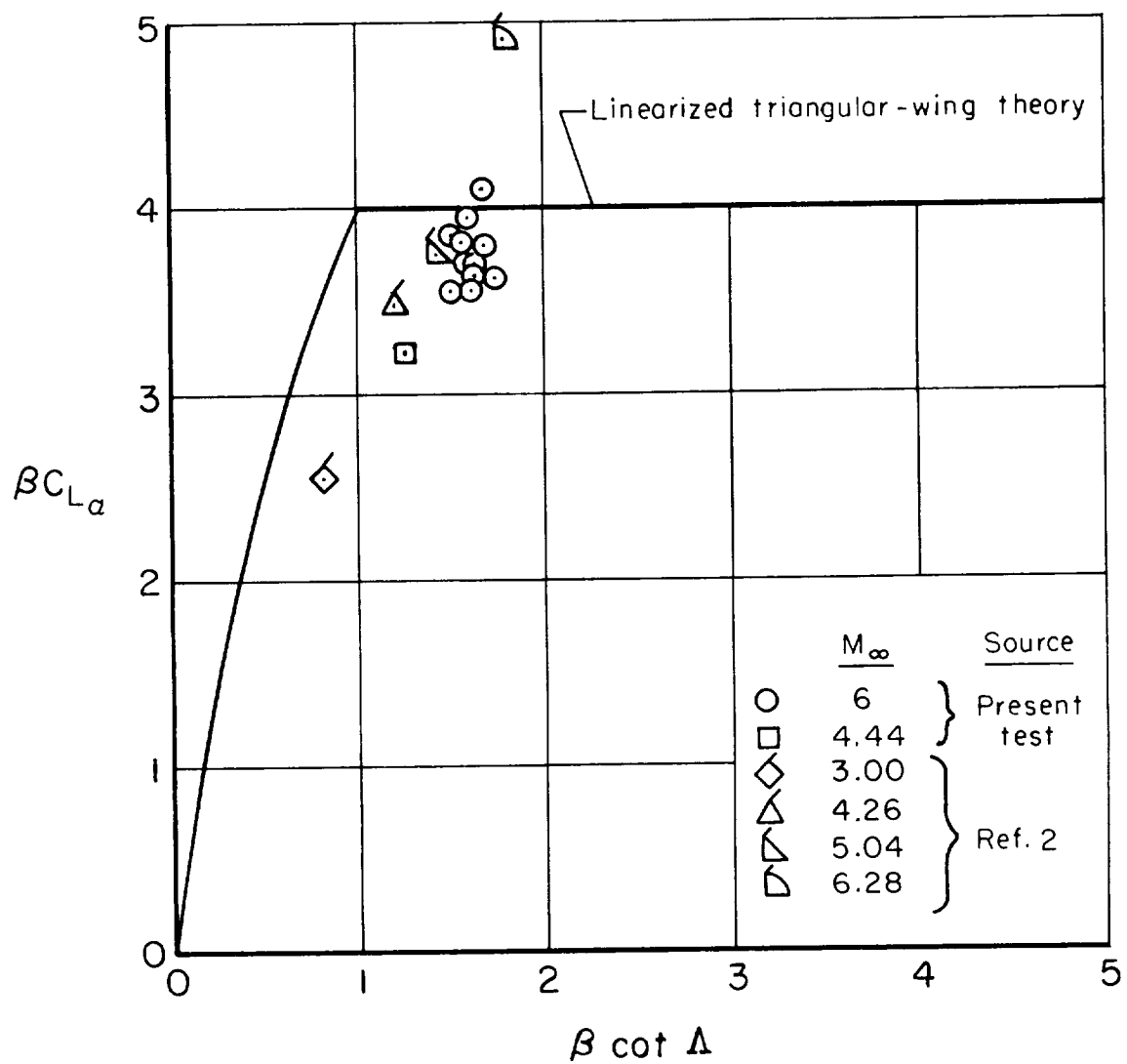


Figure 14.- Comparison of experimental lift-curve slopes with theory.

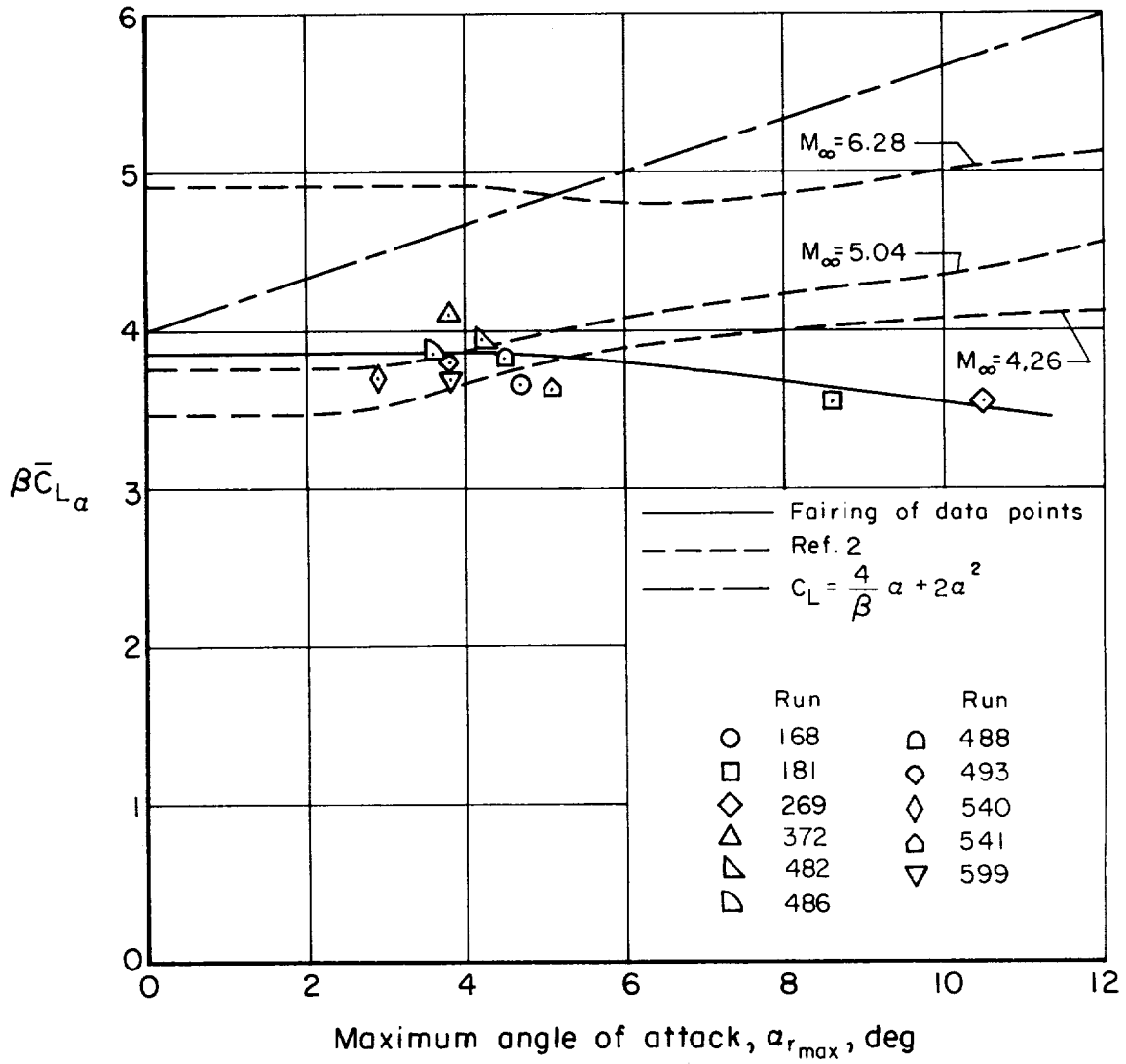


Figure 15.- Variation of $\beta \bar{C}_{L\alpha}$ with pitching amplitude.

A
2
4
0

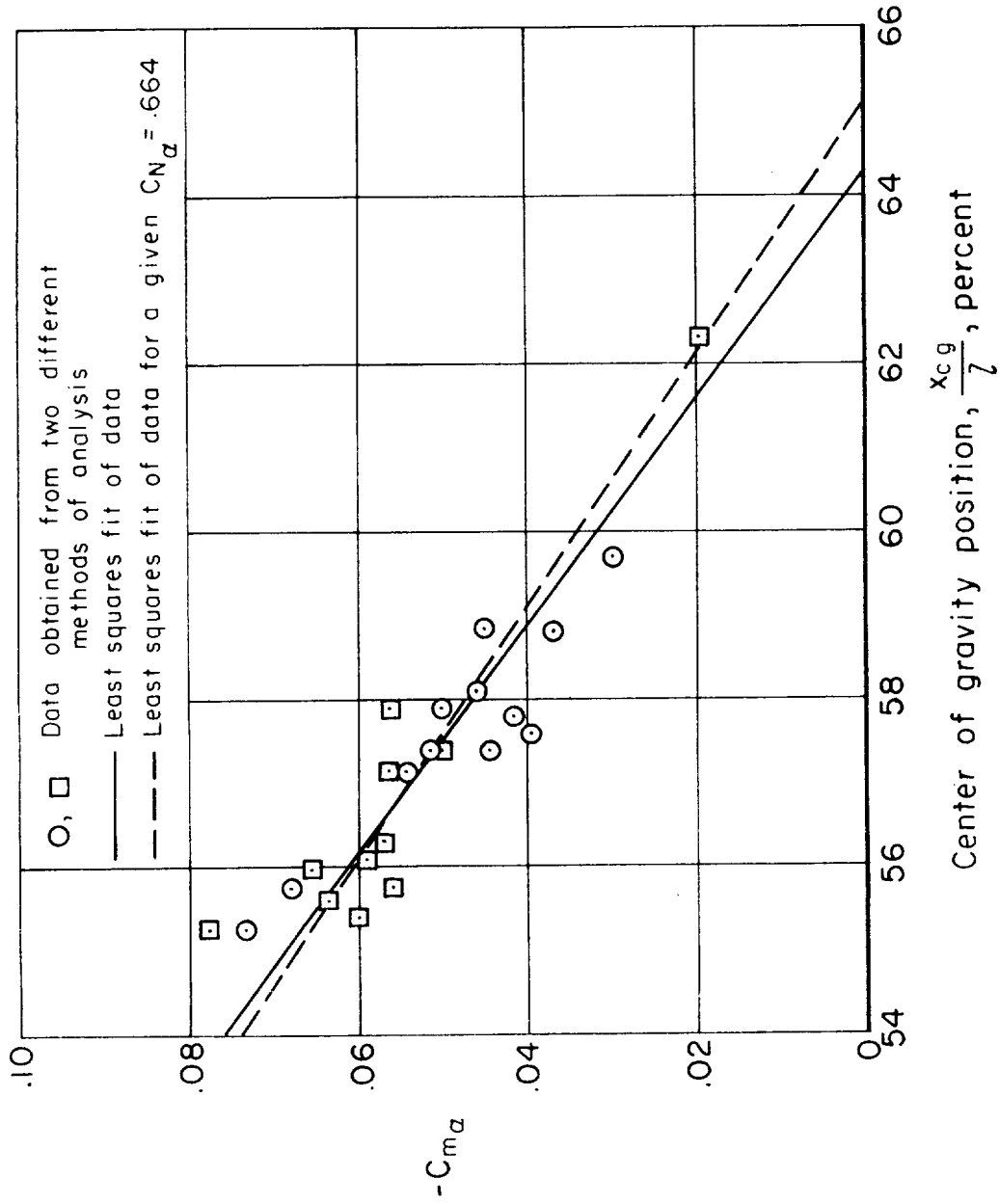


Figure 16.- Variation of moment curve slope with the center-of-gravity position; $M_{\infty} = 6.0$.

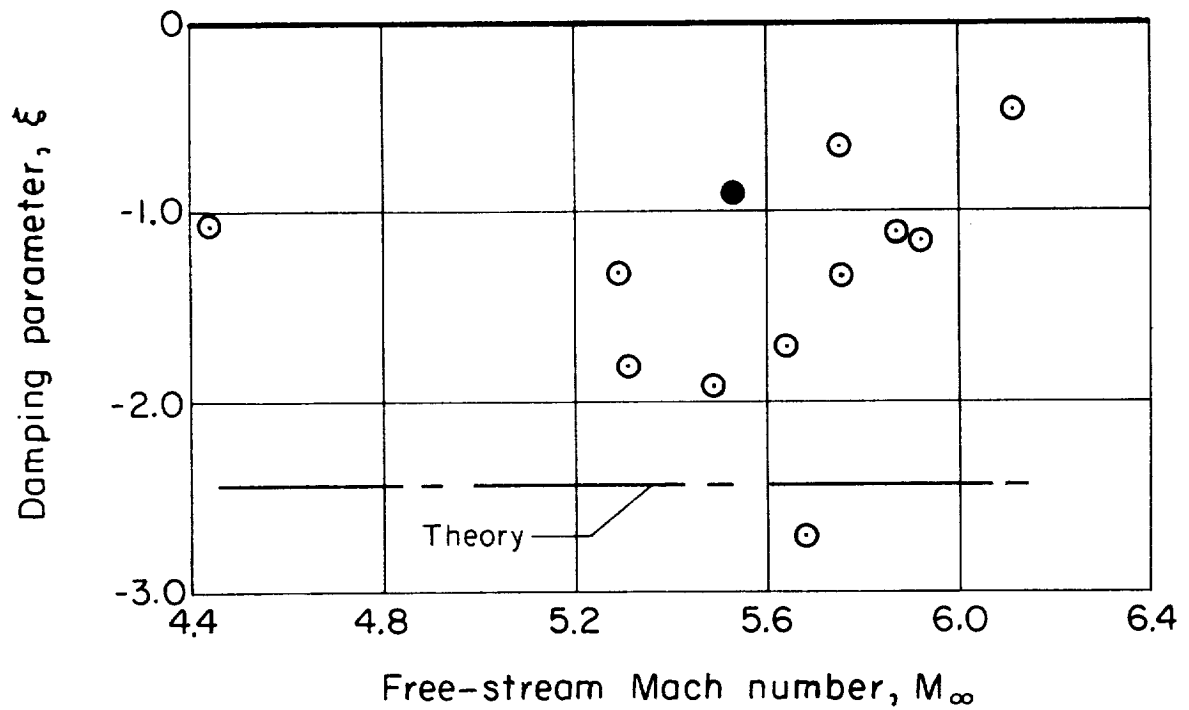
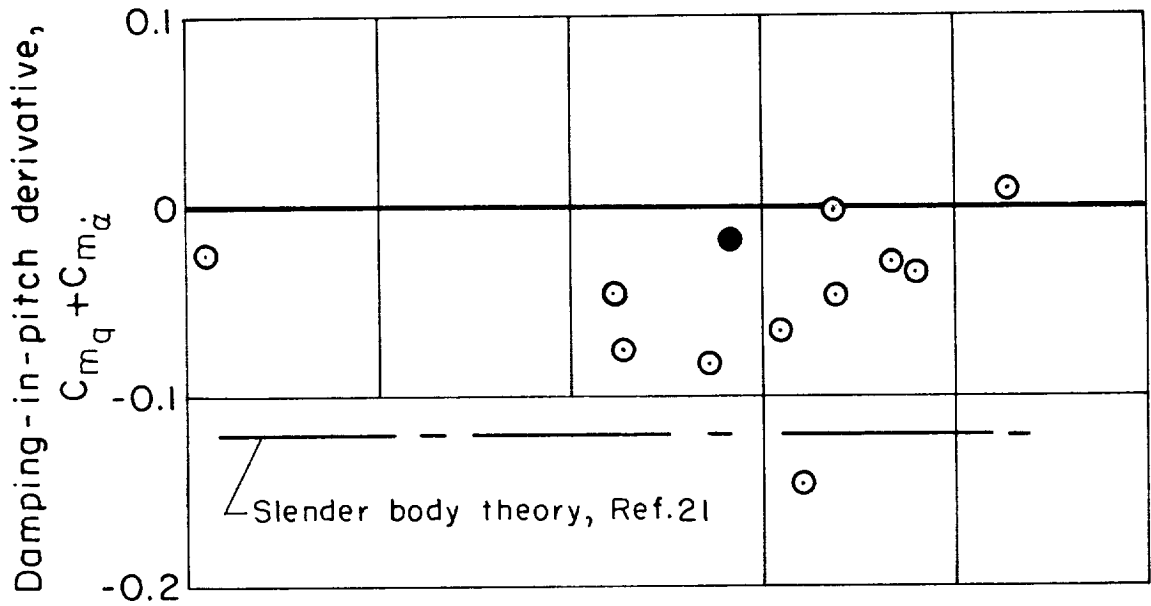


Figure 17.- Comparison of experimental dynamic stability coefficients with theory ($R_\infty \approx 6 \times 10^6$ except for filled in point for which $R_\infty = 15.7 \times 10^6$).

A
2
4
0

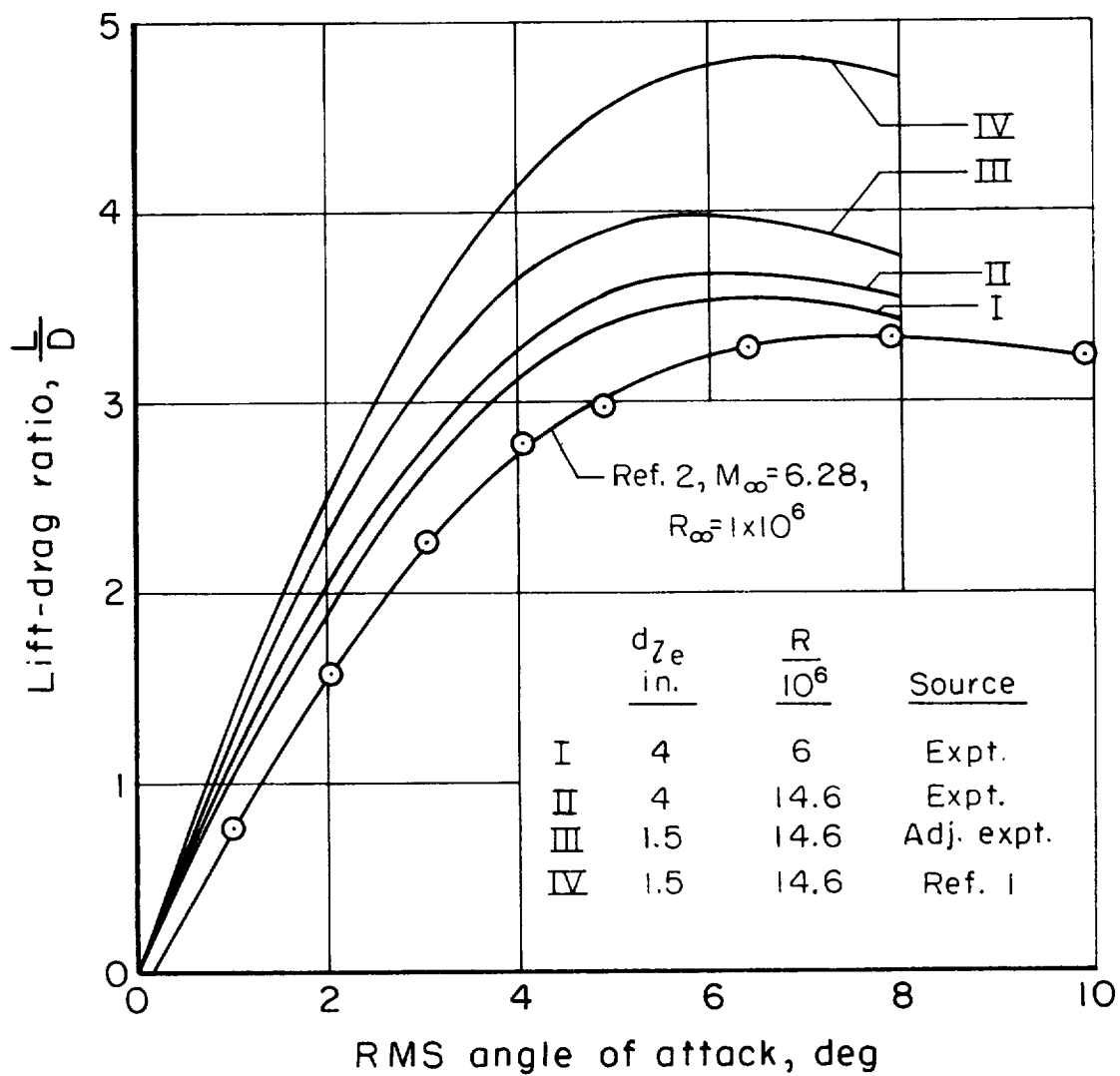


Figure 18.- Comparison of estimated L/D for turbulent boundary layer from reference 1 with smooth-model data.

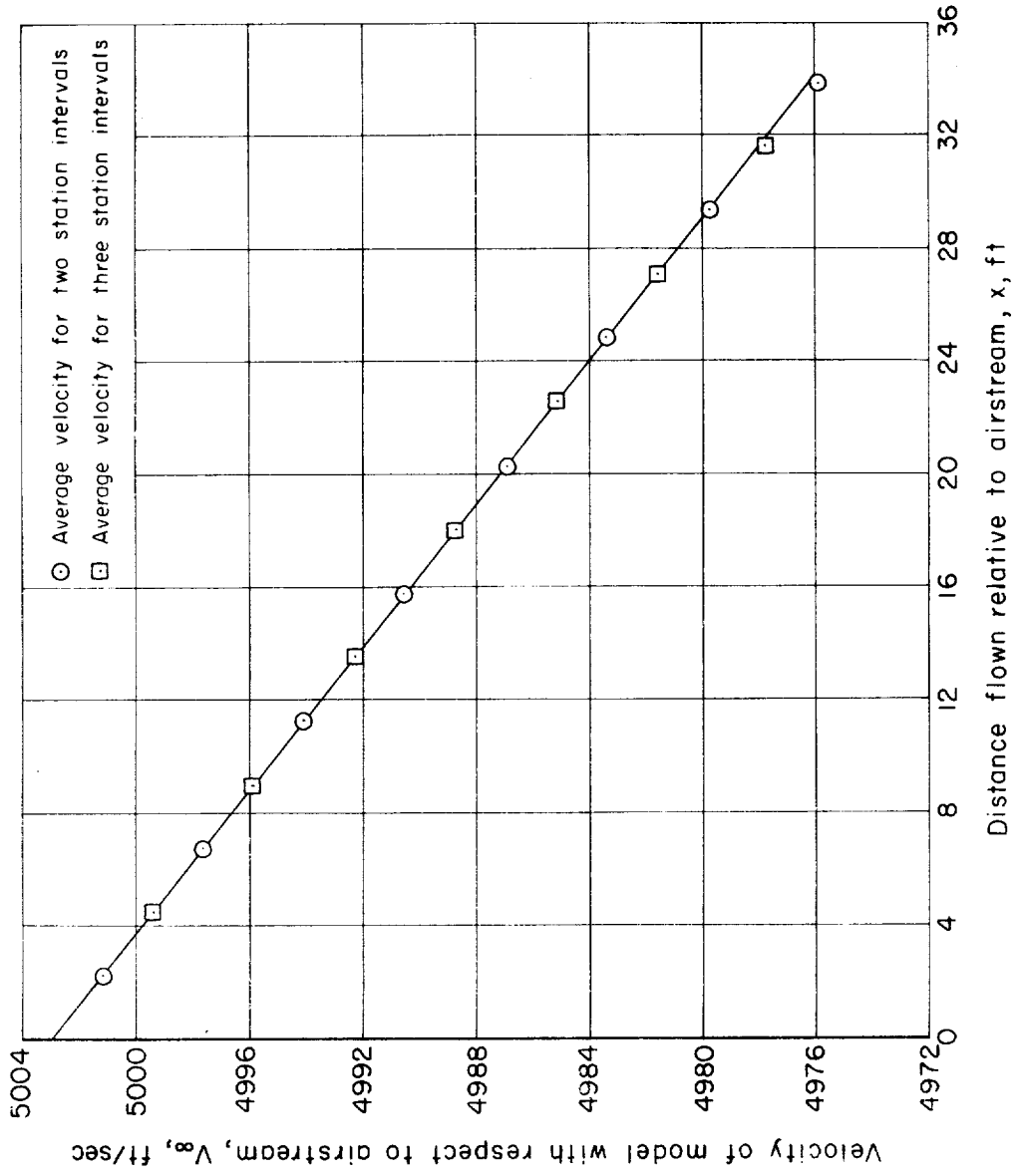


Figure 19.- Variation of velocity with distance for a model at small angles of attack ($< 4^{\circ}$).

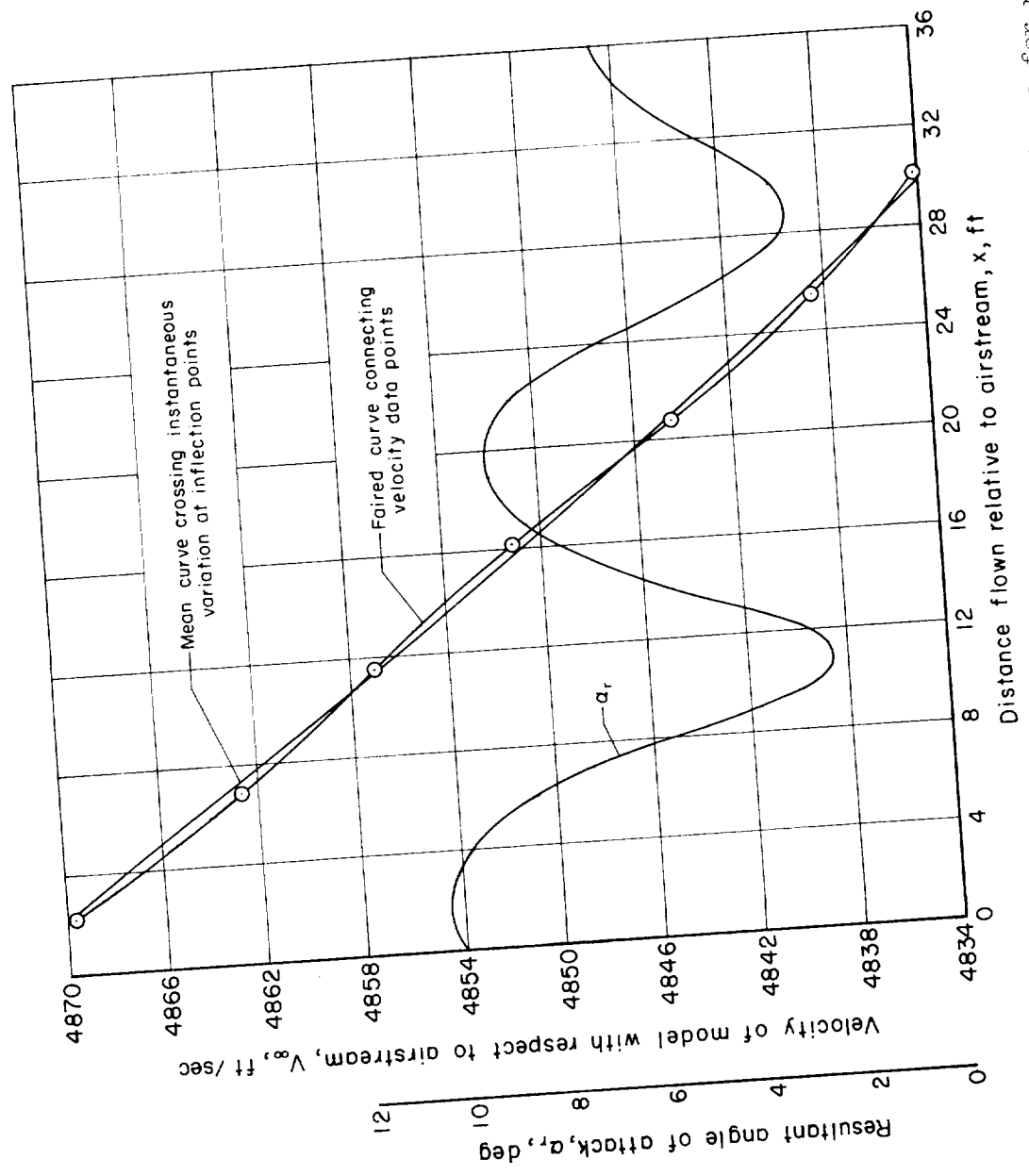


Figure 20.- Variation of velocity and resultant angle of attack with distance for run 181.



<p>NASA TN D-341 National Aeronautics and Space Administration. EXPERIMENTAL INVESTIGATION OF A HYPER-SONIC GLIDER CONFIGURATION AT A MACH NUMBER OF 6 AND AT FULL-SCALE REYNOLDS NUMBERS. Alvin Seiff and Max E. Wilkins. January 1961. 69p. OTS price, \$1.75. (NASA TECHNICAL NOTE D-341)</p> <p>A hypersonic airplane configuration consisting of three triangular wing panels and a body of equal length is investigated in tests at a Mach number of 6 and at Reynolds numbers from 6 to 16 million by use of gun-launched models. Characteristics investigated included minimum drag with rough and smooth model surfaces, lift-curve slope, and static and dynamic stability. The results are used to evaluate theoretical estimates of the configuration performance. The methods used to estimate the performance are described. The extent of laminar flow on the models at full-scale Reynolds number is determined.</p> <p>Copies obtainable from NASA, Washington</p>	<p>I. Seiff, Alvin II. Wilkins, Max E. III. NASA TN D-341</p> <p>(Initial NASA distribution: 1, Aerodynamics, aircraft; 2, Aerodynamics, missiles and space vehicles; 50, Stability and control.)</p>	<p>NASA TN D-341 National Aeronautics and Space Administration. EXPERIMENTAL INVESTIGATION OF A HYPER-SONIC GLIDER CONFIGURATION AT A MACH NUMBER OF 6 AND AT FULL-SCALE REYNOLDS NUMBERS. Alvin Seiff and Max E. Wilkins. January 1961. 69p. OTS price, \$1.75. (NASA TECHNICAL NOTE D-341)</p> <p>A hypersonic airplane configuration consisting of three triangular wing panels and a body of equal length is investigated in tests at a Mach number of 6 and at Reynolds numbers from 6 to 16 million by use of gun-launched models. Characteristics investigated included minimum drag with rough and smooth model surfaces, lift-curve slope, and static and dynamic stability. The results are used to evaluate theoretical estimates of the configuration performance. The methods used to estimate the performance are described. The extent of laminar flow on the models at full-scale Reynolds number is determined.</p> <p>Copies obtainable from NASA, Washington</p>	<p>I. Seiff, Alvin II. Wilkins, Max E. III. NASA TN D-341</p> <p>(Initial NASA distribution: 1, Aerodynamics, aircraft; 2, Aerodynamics, missiles and space vehicles; 50, Stability and control.)</p>
<p>NASA TN D-341 National Aeronautics and Space Administration. EXPERIMENTAL INVESTIGATION OF A HYPER-SONIC GLIDER CONFIGURATION AT A MACH NUMBER OF 6 AND AT FULL-SCALE REYNOLDS NUMBERS. Alvin Seiff and Max E. Wilkins. January 1961. 69p. OTS price, \$1.75. (NASA TECHNICAL NOTE D-341)</p> <p>A hypersonic airplane configuration consisting of three triangular wing panels and a body of equal length is investigated in tests at a Mach number of 6 and at Reynolds numbers from 6 to 16 million by use of gun-launched models. Characteristics investigated included minimum drag with rough and smooth model surfaces, lift-curve slope, and static and dynamic stability. The results are used to evaluate theoretical estimates of the configuration performance. The methods used to estimate the performance are described. The extent of laminar flow on the models at full-scale Reynolds number is determined.</p> <p>Copies obtainable from NASA, Washington</p>	<p>I. Seiff, Alvin II. Wilkins, Max E. III. NASA TN D-341</p> <p>(Initial NASA distribution: 1, Aerodynamics, aircraft; 2, Aerodynamics, missiles and space vehicles; 50, Stability and control.)</p>	<p>NASA TN D-341 National Aeronautics and Space Administration. EXPERIMENTAL INVESTIGATION OF A HYPER-SONIC GLIDER CONFIGURATION AT A MACH NUMBER OF 6 AND AT FULL-SCALE REYNOLDS NUMBERS. Alvin Seiff and Max E. Wilkins. January 1961. 69p. OTS price, \$1.75. (NASA TECHNICAL NOTE D-341)</p> <p>A hypersonic airplane configuration consisting of three triangular wing panels and a body of equal length is investigated in tests at a Mach number of 6 and at Reynolds numbers from 6 to 16 million by use of gun-launched models. Characteristics investigated included minimum drag with rough and smooth model surfaces, lift-curve slope, and static and dynamic stability. The results are used to evaluate theoretical estimates of the configuration performance. The methods used to estimate the performance are described. The extent of laminar flow on the models at full-scale Reynolds number is determined.</p> <p>Copies obtainable from NASA, Washington</p>	<p>I. Seiff, Alvin II. Wilkins, Max E. III. NASA TN D-341</p> <p>(Initial NASA distribution: 1, Aerodynamics, aircraft; 2, Aerodynamics, missiles and space vehicles; 50, Stability and control.)</p>
<p>NASA TN D-341 National Aeronautics and Space Administration. EXPERIMENTAL INVESTIGATION OF A HYPER-SONIC GLIDER CONFIGURATION AT A MACH NUMBER OF 6 AND AT FULL-SCALE REYNOLDS NUMBERS. Alvin Seiff and Max E. Wilkins. January 1961. 69p. OTS price, \$1.75. (NASA TECHNICAL NOTE D-341)</p> <p>A hypersonic airplane configuration consisting of three triangular wing panels and a body of equal length is investigated in tests at a Mach number of 6 and at Reynolds numbers from 6 to 16 million by use of gun-launched models. Characteristics investigated included minimum drag with rough and smooth model surfaces, lift-curve slope, and static and dynamic stability. The results are used to evaluate theoretical estimates of the configuration performance. The methods used to estimate the performance are described. The extent of laminar flow on the models at full-scale Reynolds number is determined.</p> <p>Copies obtainable from NASA, Washington</p>	<p>I. Seiff, Alvin II. Wilkins, Max E. III. NASA TN D-341</p> <p>(Initial NASA distribution: 1, Aerodynamics, aircraft; 2, Aerodynamics, missiles and space vehicles; 50, Stability and control.)</p>	<p>NASA TN D-341 National Aeronautics and Space Administration. EXPERIMENTAL INVESTIGATION OF A HYPER-SONIC GLIDER CONFIGURATION AT A MACH NUMBER OF 6 AND AT FULL-SCALE REYNOLDS NUMBERS. Alvin Seiff and Max E. Wilkins. January 1961. 69p. OTS price, \$1.75. (NASA TECHNICAL NOTE D-341)</p> <p>A hypersonic airplane configuration consisting of three triangular wing panels and a body of equal length is investigated in tests at a Mach number of 6 and at Reynolds numbers from 6 to 16 million by use of gun-launched models. Characteristics investigated included minimum drag with rough and smooth model surfaces, lift-curve slope, and static and dynamic stability. The results are used to evaluate theoretical estimates of the configuration performance. The methods used to estimate the performance are described. The extent of laminar flow on the models at full-scale Reynolds number is determined.</p> <p>Copies obtainable from NASA, Washington</p>	<p>I. Seiff, Alvin II. Wilkins, Max E. III. NASA TN D-341</p> <p>(Initial NASA distribution: 1, Aerodynamics, aircraft; 2, Aerodynamics, missiles and space vehicles; 50, Stability and control.)</p>

